Analysis of Copper Slags from the Archaeological Site of El Manchon, Guerrero, Mexico

by

Rachel Sharp

Submitted to the Department of Materials Science and Engineering in Partial Fulfillment of the Requirements for the Degree of

Bachelor of Science

at the

Massachusetts Institute of Technology

June 2003

Signature of Author..... Signature redacted
Department of Materials Science and Engineering
May 9, 2003

Certified by ..... Signature redacted
Heather N. Lechtman
Professor of Archaeology and Ancient Technology
Thesis Supervisor

Certified by ..... Signature redacted
Dorothy Hosler
Professor of Archaeology and Ancient Technology
Academic Advisor

Accepted by ..... Signature redacted
Caroline A. Ross
Associate Professor of Materials Science and Engineering
Chairman, Undergraduate Thesis Committee

Analysis of Copper Slags from the Archaeological Site of El Manchon, Guerrero, Mexico

by

Rachel Sharp

Submitted to the Department of Materials Science and Engineering on May 16, 2003 in Partial Fulfillment of the Requirements for the Degree of Bachelor of Science in Archaeology and Materials

ABSTRACT

A detailed study on metallurgical slags and ores excavated from the site of El Manchon, Guerrero, Mexico was performed to reconstruct the copper smelting process used by the ancient metalworkers of El Manchon. El Manchon is the first ancient copper smelting site to be identified in Mesoamerica. Bulk chemical analysis, electron microprobe analysis, and x-ray diffraction were carried out on excavated ores to determine their chemical composition and phase composition. Macroscopic and microscopic examination and photography were carried out on the excavated slags in order to develop a system of characterization for the slags. Bulk chemical analysis was performed to determine the chemical composition of the slags. X-ray diffraction and electron microprobe analyses were done to determine the crystalline phases present in the slags. Thermal melting experiments and calculations were carried out on slags to determine the minimum melting temperature.

Results show that the furnace charge being smelted at the site was composed of charcoal mixed with copper oxides and carbonates. The ore was primarily self-fluxing, as the ore body contained copper and iron oxides in association with rocky quartz. The furnaces most likely did not have to operate at temperatures in excess of about 1200˚C to smelt effectively. The slags produced were primarily crystalline and glassy fayalite, with a small amount of tridymite. The metal produced by the smelting operation was almost pure copper, with a small amount of iron and sulfur impurities.

Thesis Advisor: Heather Lechtman
Title: Professor of Archaeology and Ancient Technology

Academic Advisor: Dorothy Hosler
Title: Professor of Archaeology and Ancient Technology

TABLE OF CONTENTS

List of Figures and Tables

Introduction

Problem Statement

This thesis is designed to be the first phase in a full investigation into the metallurgical technologies used at the archaeological site of El Manchon, Guerrero, Mexico. We hope eventually to reconstruct the entire copper smelting process used by the El Manchon metalworkers from site data, ore, and slag analyses. The remains of smelting furnaces as well as other features of the site are in the process of being excavated. Information generated from analysis of the furnace slags will help to guide further investigation into the extractive metallurgical processes practiced at the site of El Manchon. Correlating the new excavation information with the laboratory analyses we perform is critical to refining our theories about how the site functioned.

This thesis is also intended to be useful as a slag manual to assist archaeologists and geologists in identifying features of slags in the field that may be of potential interest. In addition, the slag analytical data compiled here will provide essential information to future investigators in a laboratory setting.

Research Goals

The primary goal of this research has been to characterize the ore minerals and smelting slags excavated at El Manchon. Characterization has been carried out at a macro scale to provide a means of identifying various types of slag quickly in a field setting.

Characterization through chemical and microstructural analyses was performed to provide data that will bear upon our reconstruction of the extractive metallurgical technologies carried out at the site.

To achieve this goal, I chose a set of fundamental, identifying features that would "fingerprint" the ore minerals and slags from the site. For each feature I established one or more analytical procedures that would help generate the fingerprint.

Feature	Analytical method
Ore mineral types and associated host rock	X-ray diffraction and electron microprobe analysis: to identify ores and possible fluxing material; to provide an estimate of the contents of the furnace charge
Gross morphology of slag types	Photography (macro and micro): to produce a visual catalog of slag types for identification and comparison
Bulk composition of the various slag types	Bulk chemical analysis of the slags: to determine their overall composition, and

	to suggest whether fluxes may have been added to the furnace charge to lower the smelting temperature and to increase slag fluidity
Metal prills present in the various slag types	Bulk chemical analysis and electron microanalysis of prills and associated matte: to provide data on the composition of the metal/alloy produced during smelting and possibly about the type of mineral smelted (e.g. oxide or sulfide)
Phases present in the various slag types	X-ray diffraction and electron microanalysis: to determine the crystallinity and/or glassy nature of the slag; to suggest the range of temperatures over which the slag may have melted
Thermal properties of the various slag types	Experimental determination of slumping and/or free running temperatures of the slags: to provide the minimum

temperature to which the furnace was raised during smelting

Characterization of the El Manchon ores and slags following the regime outlined here will help us to reconstruct the copper smelting process utilized by the ancient metalworkers at this pre-Hispanic site. Ultimately, we hope this study will lead to work that establishes the technologies and the organization of metal extraction, processing, and production in Mesoamerica.

Site Description of El Manchon

El Manchon is the first ancient copper smelting site to be identified in Mesoamerica, home of the Maya, the Aztec, and other great civilizations. In 1998, Professor Dorothy Hosler found and described the site during her archaeological survey of the municipio of Coyuca de Catalan, Guerrero in the Balsas River drainage area of West Mexico (Fig. 1). Two recent radiocarbon dates indicate that the site was occupied between about A.D. 1200 and 1400, a few hundred years before the Spanish invasion of Mexico. Preliminary pottery type identification corroborates this estimate; the presence of Balsas Red and Yestla Naranjo pottery indicates that the site was occupied in the late Postclassic period, a time period that includes the absolute dates previously mentioned.

El Manchon is located 1.4 km from the Sierra Madre del Sur and is 2.5 km southeast of the modern town of Altamirano. It is situated at about 1400 m above sea level on a small

tributary of the Balsas River (Fig.2). It is comprised of one large copper smelting area and two immediately adjacent areas of habitation. From what is currently known about the site, it is most likely the ancient equivalent of a mining and ore processing camp. The living area is small and directly associated with the smelting installations, yet cultural material associated with the site is distributed in a 3 km^2 area around the primary structures. The domestic ceramics found at the site reinforce an interpretation that a wide range of activities besides smelting was carried out there. The surrounding area is not suitable for agriculture, as the layer of fertile soil is shallow and eroded due to deforestation. People working at this site could not have supported themselves without resources from outside (Dorothy Hosler, personal communication, 2003).

El Manchon lies within the West Mexican Metalworking Zone, a region characterized by a high density of copper ore deposits (Fig. 2). The copper mine associated with its smelting operations has yet to be located on site survey. Small deposits of copper ore occur frequently in the vicinity of El Manchon, so we are confident that the primary source of ore is not far removed from the site. The smelting sector at the site covers an area of 40 x 50 m^2. A series of small stone smelting furnaces is located within this area. Unfortunately, the furnaces have been heavily disturbed by the roots of trees growing in close association with these ancient features.

The smelting sector is distinguished by the large accumulation of slag that follows inside the course of a seasonal streambed. In early 2001, Professor Hosler and her team excavated the slag studied in this thesis from a specific feature. This feature is a large

slide of slag (approximately 2 meters long) located down the side of a precipitous hill slope. The slag appears to have collapsed from a large pile at the top of the slope, and then slid down the side (Jenkins 2001).

Metallurgy in the New World

The first known metallurgical operations in America can be documented to about 1500 B.C., occurring in the Central Andes region of South America (West 1994). This is in contrast to the first discovery and use of metal in the Old World. Cayönü Tepesi, a site in northwest Turkey, has yielded early metal artifacts dated to the eighth millennium B.C. (Todd 1976). In the Americas, native gold, native copper and copper carbonate ores collected from surface deposits were initially used in the production of metal objects. Eventually binary alloys such as Cu-As, Cu-Sn, Cu-Au, and Cu-Ag, and ternaries such as Cu-Au-Ag and even Cu-As-Ni were used in the manufacture of objects from metal. The development of these alloys as well as the smelting of sulfide ores occurred in the Central Andes region (Lechtman 1979, 1988, 1996, 2002). The primary mode of shaping metal in the Andean region was through the manipulation of metal sheet, working the metal in its solid state.

Various cultures in South America participated in the development of metallurgical technologies. The Chavín religious cult in Peru disseminated religious paraphernalia in the form of beaten gold objects from about 1000 to 200 B.C. (West 1994). Later, their successors, the Moche, brought metalworking in South America to its most sophisticated

level (Lechtman 1984). They perfected the use of Cu-Ag, Cu-Au, and Cu-Ag-Au alloys and formed them into metal sheet from which three-dimensional objects were elaborated. Items such as rattles of sheet metal were joined with solder. The solder, often a Cu-Ag alloy, melted at a lower temperature than the sheet it was joining, so the Moche could use the liquid metal to join solid metal parts composed of a different alloy with a higher melting temperature (Lechtman 1991). The Chimú, in turn, followed the Moche and used the techniques developed by them to build such a well-respected reputation for metalwork that the Inka brought them to work at the royal court in Cuzco. The Chimú, and the Sicán peoples before them, were responsible for developing arsenic bronze, the binary alloy of copper with arsenic that dominated Central Andean metallurgy until the Inka conquest of the region (Lechtman 1993; Shimada 1985). The Inka imposed a large amount of influence on Andean regional metalworking by enforcing the use of tin bronze (Cu-Sn alloy) as preferable to the arsenic bronze traditionally used.

A different type of metalworking tradition arose in the region of present-day Colombia, to the north of the Central Andes and, slightly later, in lower Central America. Around 100 A.D., peoples in the Colombian area established a metalworking tradition based on casting, as opposed to working metal. Casting, in this case using the lost wax method, employs metal in its liquid phase. In addition, this casting technology predates the appearance of casting in West Mexico (Hosler 1994).

West Mexican metallurgy took aspects of both types of metalworking and synthesized them into a metalworking tradition different from either progenitor (Hosler 1994). Early

artifacts from Period I of the West Mexican metalworking tradition (A.D. 500-12/1300) are virtually identical in form and methods of manufacture to their counterparts in Ecuador, the North Peruvian Andes, and Colombia. Open rings, perforated-eye needles, beam design tweezers, axes, awls, fishhooks made from copper and low arsenic Cu-As alloys were made in West Mexico using the same fabrication techniques as those in Ecuador. The West Mexican artifacts are also found within analogous archaeological contexts as their counterparts in Ecuador (Hosler 1994). The method of fabricating 'blanks' for fishhooks, needles, and awls in West Mexico is the same as that used in the Andean region. These were shaped using solid deformation techniques rather than by casting. During Period I of West Mexican metalworking, the bells manufactured in West Mexico were identical in both their overall design and fabrication method to the types of bells made in Colombia, Costa Rica, and Panama. These bells, all cast using the lost wax method, have a suspension ring attached and contain a clapper (Hosler 1994).

The most accepted theory for the transfer of metallurgical technology to West Mexico from regions far to the south argues for a maritime route involving the sea-faring peoples of coastal Ecuador (Hosler 1994) (Fig. 3). The metallurgical techniques used in both Ecuador and West Mexico at this time are virtually unknown in the intervening landmass between the two regions. Thus it seems unlikely that the knowledge was transferred overland. The only other reasonable method of knowledge transfer between the two regions is via Pacific Ocean routes. Nor is there any evidence from southern Mesoamerica to support the diffusion of knowledge of casting operations overland from Colombia. A Pacific coastal maritime route is suggested for this knowledge spread as

well (Hosler 1994). The trade good that seems to have sparked the long-distance maritime expeditions of the Ecuadorian peoples is the *Spondylus princeps*, the highly colored shell of a marine animal that lives in the warm equatorial waters of the Pacific and is found abundantly off the coasts of Ecuador and West Mexico (Hosler 1994). *Spondylus* shell and items made from it was probably the most highly valued ritual material traded into the Andean culture area.

The earliest appearance of copper in West Mexico is at the site of Tomatlán, Jalisco. The metal objects excavated there bear resemblance to objects from both Ecuador and Colombia. Yet cast bell, probable needle fragment, awl-like item, fishhook and two metal strips were made in West Mexico, not imported. It is argued that the artifacts were replicated from Andean models by the West Mexican artisans. The West Mexicans clearly imported technological knowledge from the south, not merely physical artifacts. For them to have designed their own metallurgical operations, they required knowledge of ore types, smelting technology, fabrication technology, and a sense of the kinds of objects it was appropriate to fashion from metal (Hosler 1994).

Period II in West Mexican metallurgy (A.D. 12/1300 to the European Invasion in 1521) was characterized by experimentation and diversification of the Period I metals and objects (Hosler 1988a, 1988b, 1994). The almost exclusive use of copper characteristic of Period I changed dramatically in Period II, as the West Mexican metalworkers experimented with tin bronze and arsenic bronze as well as a Cu-Sn-As ternary alloy. The technologies behind the production of these alloys were, again, introduced from the N.

Andean region. Artifact types diversified from those present in Period I into new subcategories. In addition, new artifact types appeared, including sheet metal and cast ornaments, and axe-monies (Hosler 1988a, 1988b, 1994; Hosler, Lechtman, and Holm 1990).

West Mexicans made massive numbers of bells relative to the peoples from whom they imported metallurgical knowledge. The sounds of the bells were important in three aspects of the sacred life of most Mesoamerican societies (Hosler 1994, 1995). The clear, high-pitched tone of the bells was used in celebrations related to fertility and regeneration, as well as to protect warriors on the battlefield. In addition, the bell sounds corresponded to the song of birds and of deities in the sacred paradise (Hosler 1994, 1995). The sounds of metallic bells were quite unlike those of the more traditional, non-metallic rattles Mesoamerican peoples employed, and these metallic sounds likely contributed to the popularity of this particular application of metallurgical technology to West Mexican religion.

Though the technologies were imported, the sacred and ritual metal items of the Andean exchange partners were not used in trade. For this reason, we do not see in Mexico the sacred bimetallic masks and pendants so revered to the south. Items deemed more secular were brought along for trade, though. The West Mexicans were thus free to superimpose their pre-existing religious ideas and cultural values onto the artifacts they manufactured using the new metalworking technology. Since they were not introduced to metal in the context of the religions practiced by S. American peoples, they did not come in direct

contact with such practices as a result of the metal trade and were largely unaffected by them (Hosler 1994).

The use of metals in the New World was symbolically associated with the gods (Hosler 1994). Gold and silver were identified with the sun and moon deities, respectively. The gods wear bells in many examples in which they are depicted in Mexican codices. Elites could thus be identified with the gods by wearing similar metallic decorations. In this way, metal became the prerogative of the elite class. It follows that the two primary interests of the West Mexican metalworkers with respect to the properties of metal were the sounds and colors of their alloys (Hosler 1994). If the color of metal provided an association between it and the gods, it would make sense that particular colors would be deemed most desirable and thus be sought after in alloys. Pure copper is a deep red color. Arsenic added to the copper, even in small amounts, will produce color variation. For example, arsenic at a concentration of 3.5% by weight will turn copper a pale pink and at a concentration of 7% will impart a silvery white color to the alloy (Hosler et al. 1990). The desire to produce culturally desirable sound and color properties from copper alloys was what drove metallurgy in the West Mexican Metalworking Zone.

Prior published research on the analysis of ancient smelting slags

An exhaustive bibliography of pertinent literature is not being presented in this thesis. Several key studies of ancient copper smelting slags from the Old World and the New World have been chosen as representative of the state-of-the-art studies of archaeological

copper smelting slags. There are no prior published studies of archaeological smelting slags from Mesoamerica. El Manchon is the first extractive metallurgical site to be identified and studied archaeologically, thus the slag investigation detailed in this thesis is the first such study to have been conducted on Mesoamerican metallurgical slags.

New World

In the Andean region of South America, where metalworking first developed in the New World, there are published studies of smelting slags from only two sites. Though the slag studies for the sites of Batán Grande, in northern Peru, and Ramaditas, in northern Chile, are not comprehensive, they are important because the smelting furnaces were found and excavated at both sites (Graffam, et al. 1994, 1996; Merkel and Shimada 1988; Shimada, et al. 1982, 1983).

Merkel and Shimada report on studies of the copper smelting slags excavated at the N. coast Peruvian site of Batán Grande (A.D. 850 – 1200). Intact bowl furnaces were excavated at the site. Bulk analyses of the slags are reported, though the analytical methods used to arrive at these results are not specified. The slags are iron silicates with moderate concentrations of alumina and lime. They contain prills of copper-arsenic alloy that were studied (presumably) with the electron microprobe. The prills contain inclusions of matte (CuFeS). The melting temperatures of the slags are not reported. They are termed "furnace slags", after Bachmann's classification system (Bachmann 1982).

Graffam, Rivera and Carevic report on evidence for copper smelting at N. Chilean sites during the first centuries BC (Graffam, et al. 1994, 1996). Furnaces and small amounts of slag were recovered. The slag was analyzed by x-ray fluorescence techniques. The slags are of two varieties: (1) high silica, low iron, and (2) silica with iron and calcium fluxes. It is not clear whether the fluxes were added intentionally or if the ores were self-fluxing. No microscopic work is reported on these slags nor were their melting temperatures determined. The copper content of the slags ranged from 0.9 to 8.0%, by weight.

Old World

Far more work on smelting sites and metal processing has been carried out on Old World sites. I am reporting on the major studies of slags in the Near East and the Mediterranean. Furnaces have been uncovered at some of the sites, but in many only the slags are still in evidence. The studies I have chosen contain the most comprehensive examinations of the slags. Several studies determined the lead isotope ratios of the slags and compared them to the lead isotope ratios of ores at the sites, with the hope that the slags could be related definitively to an ore source. The earliest and undoubtedly most influential of these works is Bachmann's (1980) report on slags from the Sinai and Negev. This provided the foundation for most subsequent analytical studies of archaeological slags. His 1982 publication was a more comprehensive, manual-style compendium of smelting slag microstructures and analyses.

Near East

Bachmann (1980) investigates early copper smelting techniques in the Sinai and in the Negev through his analysis of their slags. This work provides the most thorough treatment of the analysis and interpretation of archaeological slags produced during early copper smelting activities and presents a scaffold or framework for the design of subsequent slag studies (such as this thesis). The study deals with smelting sites in the Sinai Peninsula and in the Timna region of present- day Israel. The materials date from the 4th millennium BC to the Roman period. This research led to Bachmann's later (1982) manual for the analysis and interpretation of slags found in archaeological contexts.

Following Bachmann's (1980) work, Segal, Rothenberg, and Bar-Matthews (1998) investigated smelting slags from Timna, SW Arabah, Israel. The site of Timna is arguably the most significant copper smelting region in the Near East. It includes a vast array of smelting furnaces from different time periods; many ancient peoples took advantage of the large ore deposits. Segal et al. investigated two prehistoric sites: Site F2, dating to the Late Pottery Neolithic Period (6th-5th millennium BC) and Site N3, dating to the Chalcolithic Period (early 4th millennium BC). These are some of the earliest copper smelting sites known archaeologically from the Near East. Fluxes were not added to the charge at the early F2 site, but iron fluxes were added to the furnace charges at the later F2 site. The investigators followed the slag analytical scheme set out by Bachmann (1982) and determined bulk chemical composition, mineral constituents, micro-petrographic and mineral chemistries on slag phases.

Hauptmann (1989) investigated copper smelting slags dating to the Chalcolithic Period (second half of the 4th millennium) and the early Bronze Age from Feinan, Jordan. Bulk chemical analyses were carried out as well as mineralogical identification of phases in the slags. The later slags were self-fluxing, with MnO as the primary flux contributed by the ore. The texture of the Chalcolithic slags indicates a smelting process capable of only partially melting the host rock in the furnace charge.

Cyprus

Stos-Gale, Maliotis, and Gale (1998) conducted a survey of Cypriot slag heaps. The slags studied range in date from the 7th century BC to about AD 480; no Bronze Age slags were analyzed. This investigation focused on comparing the lead isotope analyses determined for Cypriot copper ores with the lead isotope analyses of the archaeological smelting slags.

Rapp Jr. (1998) investigated the composition and softening/fluid temperatures of ancient Cypriot slags. The primarily Bronze Age slags were crushed, made into pyrometric cones, then heated in an ash fusion furnace and the temperatures of softening and melting were recorded.

Zwicker, Greiner, Hofmann, and Reithinger (1985) discuss the evidence for crucible copper smelting in the ancient Near East. Slag adhering to the wall of a Cypriot crucible was examined with the electron microprobe. It contained copper prills with sulfide

inclusions. Cu-Fe-S inclusions were also identified within the matrix of the slag. These materials date to the Late Bronze Age.

Cycladic Islands

Stos-Gale (1989) examined ores and slags from several of the Cycladic islands. The metallurgical remains date to the 3rd millennium BC, the Aegean Early Bronze Age. The slags were analyzed by the electron microprobe. They contain copper prills and are of the fayalite type. Lead isotope analyses of the ores and slags were also carried out. A radiocarbon analysis of charcoal from the slag dates the slags to 2800 – 2500 BC.

In general, few extractive metallurgical sites have been found and studied by archaeologists anywhere in the world. In particular, comprehensive studies are rare. The investigation of the slags from these sites has been carried out by a handful of individuals.

The Ore Geological Context

Metal Ores

West Mexico includes the modern states of Sinaloa, Nayarit, Jalisco, Colima, Michoacan, Guerrero, and Estado de Mexico as shown in Figure 4.Within the limits of West Mexico there is a rich region of metallic ore deposits. Hosler has identified this area as the West Mexican Metalworking Zone (Hosler 1994). It is the region where metallurgy first developed in Mesoamerica. The site of El Manchon in located within this region.

Numerous deposits of copper, arsenic, tin, lead, and silver are found in this zone, either as native metal or metallic ore and, in some cases, both. For the purposes of this thesis, I will concentrate on copper deposits. There are two distinct loci of copper ore concentration within the metalworking zone; one is to the northwestern side of the region, including western Jalisco, Colima and Nayarit (Fig. 4). The other is to the southeastern side of the region, including the states of Mexico, eastern Michoacan, and western Guerrero (Hosler 1994). El Manchon, in western Guerrero, lies within the southeastern copper deposit region (Fig. 4).

A number of various copper ores can be found within these deposits. Primary sulfide ores of copper-containing minerals such as chalcopyrite ($CuFeS_2$) and chalcocite (Cu_2S) are common. Carbonate and oxide ores of copper are also found, such as malachite [$Cu_2(CO_3)(OH)_2$], azurite [$Cu_3(CO_3)_2(OH)_2$], and cuprite (Cu_2O). Copper is also present in its native metal form. Additionally, copper occurs in complex minerals that contain other metals. Enargite is a copper sulfarsenide (Cu_3AsS_4) that can be processed to yield copper-arsenic bronze alloys. In the deposits of West Mexico, copper generally appears as a sulfide ore (Hosler 1994).

Wherever metal sulfide deposits exist, metal oxides generally accompany the primary sulfides. Oxides are usually the weathered products of the sulfide ores. In the case of El Manchon, microscopic examination and electron microprobe analysis of cross-sections through some metal oxide ores excavated there revealed small remnants of the original sulfide ore contained within the weathered oxide product (See **Results: Ore Analyses**).

The weathering of ores depends on both physical and chemical changes. Physical changes are related to mechanical processes within the earth's crust, such as tectonic activity, as well as wind erosion and other surface processes that break down the exposed ore body. Chemical changes are induced by the presence of groundwaters that dissolve sulfide ores to form acid solutions that interact with other mineral compounds. Minerals can be modified chemically, leached from a mineral deposit, and/or deposited from one zone to a different location in the mineral deposit, as shown in Figure 5 (Dietrich and Skinner 1979; Allen et al. 1990).

A vein of sulfide mineral, when exposed to surficial conditions, becomes modified over time by these weathering processes. Ground waters dissolve pyrite (FeS_2) to form sulfuric acid (H_2SO_4) as well as various iron oxides (gossans). The sulfuric acid dissolves metallic minerals creating sulfate solutions that leach out of the surface layers and travel deeper into the mineral vein, where they may deposit various native metals, oxides, carbonates, silicates and sulfates. These oxide minerals are located above the water table and, thereafter, are easier to access. Below the water table, which is an oxygen-free saturated zone, these percolating solutions interact with the primary sulfide ores, enriching them. These ores, located in the enriched zone of deposition, are known as supergene ores. They tend to become enriched in non-ferrous metals, such as copper that have a greater affinity for sulfur than iron, which is replaced in the ore by the non-ferrous metals (Dietrich and Skinner 1979; Chernicoff and Whitney 2002).

We believe that the ores smelted at El Manchon were oxide ores of copper that contained iron and were likely hosted within silica-rich hydrothermal quartz veins. The analyses of the El Manchon ores are treated in the section **Results: Ore Results**.

Principles of Extractive Metallurgy and the Formation of Slag

Smelting and the Formation of Slags

The goal of extractive metallurgy is the winning of metal from a metallic ore. Smelting of oxide ores in a furnace under reducing conditions was the most common extractive metallurgical practice throughout the pre-industrial world. In ancient times this was accomplished by charging the furnace with ore and fuel (usually charcoal) and heating the fuel to produce a reducing environment. When oxide ores comprised the charge, the reducing gases eliminated the oxygen content of the ore, leaving the metal to collect in the furnace bottom (see Fig. 6). The non-metallic portions of the ore – the rocky gangue – were eliminated in the form of slag, which floated above the smelted metal.

The Fundamental Chemical Reactions of Reduction Smelting

Reduction smelting can be used to remove copper from its oxide ores (Lechtman and Klein 1999). In the reaction given here the equation is balanced, but the mineral formulae do not represent stoichiometric components.

$$\underset{\text{copper carbonate}}{CuCO_3} + \underset{\text{carbon monoxide}}{CO\uparrow} \xrightarrow{\text{heat}} \underset{\text{copper metal}}{Cu} + \underset{\text{carbon dioxide gas}}{2\,CO_2\uparrow}$$

The reaction occurs in the presence of a reducing atmosphere created by the partial burning of charcoal to produce carbon monoxide. The mineral ores used in metal production are not pure copper carbonates. Typically, they contain impurities. In addition, ores are mined in association with assorted gangue, the rocky non-metallic minerals that are eliminated by slag formation during the smelting process. Occasionally the gangue associated with the ore can be of appropriate composition to serve as a flux for the ore, for example if the gangue contains sufficient silica or iron oxides. These are called self-fluxing ores, and, when smelted, can induce slag formation without an additional flux component. More complicated reactions are associated with the winning of metals from sulfidic ores. Whereas these kinds of operations certainly occurred in prehistory, all the archaeological evidence at the site of El Manchon indicates that the more weathered, oxide ores were utilized.

Slag

During smelting, it is desirable to form a slag within the furnace. Slags act as collectors of impurities (that is, non-metallic entities), which are always present in a smelting operation due to inevitable natural variations in ore composition, the presence of gangue materials from the rocky matrix in which the ore was emplaced, inclusions from the furnace lining, and charcoal/charcoal ash. Slags scavenge these impurities and aid in

purification of the metal. An understanding of the nature of slag formation is essential for any investigation into the technological aspects of a smelting site.

Since an ore is comprised of a metallic mineral in association with the rocky matrix in which it formed, this rocky material (gangue) must be eliminated during the smelting process. It is most readily removed as a slag. Metallurgical slag is defined as the vitrified material waste resulting from the smelting of metal ores. Slags are fused oxides; they are silicates formed by the fusing of silica (SiO_2) and metallic oxides. Metal oxides (from metallic minerals which were not completely reduced to metal or that were added as a flux) such as wüstite (FeO), as well as other trace oxides like Al_2O_3 and MgO, may be present. Additionally, minerals such as fayalite ($2FeO{\cdot}SiO_2$), monticellite ($FeO{\cdot}CaO{\cdot}SiO_2$), akermanite ($FeO{\cdot}2CaO{\cdot}2SiO_2$) and pyroxene ($FeO{\cdot}CaO{\cdot}2SiO_2$) can be present, typically in large amounts. These heat-created minerals consist of iron oxide (sometimes with substitutions of zinc, magnesium, and/or manganese oxides) combined in specific proportions to SiO_2 and CaO (Bachmann 1982). Fayalite is one of the most common constituents of early slags and is desirable because of its low melting temperature (see Fig. 7.)

Slag can be glassy, crystalline, or a combination of both, and is mostly siliceous in composition. Slag fluidity is an important factor to determine from ancient metallurgical operations, as it is an indicator of technological efficiency. A slag of low viscosity (low SiO_2 content) allows the smelted metal to sink through it under the influence of gravity and to form an ingot at the base of the furnace. In such cases the slag floats above the metal, being of much lower density (see Fig. 6). A higher viscosity slag (high SiO_2

content) traps metal prills within it. Upon solidification, such slag must be broken and crushed to recover the prills, which are consolidated through remelting (Shimada et al. 1982, 1983; Graffam et al. 1994, 1996). Thus the smelting process has both chemical and physical components. Separation of metal from ore depends upon the chemical reduction of the ore followed by physical separation of the metal from the slag.

Extractive metallurgical installations in the ancient Andes, S. America

Metallurgical operations that demonstrate either the viscous or the fluid slags are in evidence in the New World. At the site of Batán Grande in Peru (ca. A.D. 850-1300), metalworkers did not achieve adequate separation of slag and metal during the smelting process (Shimada et al. 1982, 1983). They used blowpipes powered by the human lung to elevate the temperature of the burning fuel (see Fig. 6) but were unable to reach temperatures high enough to melt the slag. The copper prills trapped in the slag were subsequently removed by crushing with large stones (batanes). The site of Ramaditas in Northern Chile (ca. 500 B.C. – A.D. 300) exhibits evidence of a more efficient smelting process, where a highly fluid slag allowed consolidation of a majority of the copper that migrated through it (Graffam et al. 1994, 1996). It is thought that wind-powered furnaces were used to achieve the elevated temperatures.

Categories of ancient slags

Different types of smelting operations yield different types of slags. Bachmann (1980) has defined several categories of ancient copper smelting slags. A *furnace conglomerate*,

the product of an early step in the conversion of ore to metal, is a collection of fused material, containing partly decomposed ore and gangue particles, charcoal fragments, and copper prills. It is not quite modified enough to be a true slag but is held together by a 'slaggy' matrix. Equilibrium (and thus slag formation) has not been achieved in these examples. A *furnace slag* is a genuine slag but still may contain evidence of the original charge. This slag type still retains a high percentage of copper within it. Because of its relatively high viscosity the copper prills remain trapped within the slag. Furnace slags must be crushed to allow for the recovery of the metal. The next level, *tapped slags*, can come in two types: fayalite ($2FeO{\cdot}SiO_2$) and knebelite [$(Mn,Fe)_2SiO_4$]. The primary difference between these two types lies in their composition. The former is found in association with medium-sized furnaces and is much more free flowing than the furnace slags. The knebelite slags are usually associated with larger-sized furnaces and are found primarily as large cakes of tapped slag. The category *tapped slags* represents a higher level of metallurgical operation, with almost perfect separation of slag and metal and high efficiency (Bachmann 1980). There are also *crucible slags*, which are often the product of the high-level refining of metals. These slags are not necessarily abundant and can vary a great deal, depending on formation circumstances.

Slag properties and the use of flux

Several qualities are desirable in the formation of slags such as low energy of formation as well as a low melting temperature. Slags that melt at relatively low temperatures

conserve fuel. In Figure 7, it is clear that the range of slag compositions that results in the formation of fayalitic slags occurs at temperatures between about 1178 and 1300°C.

The Central Andean method of using blowpipes to increase the furnace temperature in the furnace (See Fig. 6) was barely sufficient to attain temperatures in the 1200°C range (Rehder 1994; Lechtman and Klein 1999). In smelting operations performed in the ancient Americas, the slag formation temperature was limited primarily by the rate at which oxygen could be introduced to the burning fuel. Bellows were not invented in the New World. In the Old World, by contrast, skin bellows were used to provide more oxygen and to raise the furnace temperature.

Smelters also strove for a high degree of fluidity in their slags so as to increase the mobility of the metal prills within the slag matrix. They often added fluxes to the furnace charge to decrease slag-melting temperatures and to increase slag fluidity. This ensured maximal separation of metal from slag. The primary fluxes employed were iron oxides, calcium carbonate (crushed limestone), and silica (as sand), to provide FeO, CaO and SiO_2 to the slag. If there is too high a concentration of SiO_2 in a slag one adds FeO or CaO as a flux; if there is too much FeO in a slag, one adds SiO_2 as a flux (e.g. see Fig. 7). Flux is a component of the charge added to facilitate the formation of a slag. Addition of an appropriate flux creates a suitable proportion of fusible oxides for the formation of slag in the furnace. Ores can have widely varying compositions. Depending on composition, an ore deposit may contain certain flux requirements, such as a good ratio of SiO_2 to FeO, to create a fusible slag. Such ores are deemed "self-fluxing". Slag

formation is dependent on the composition of the smelting charge as well as on the furnace construction and its operation (Bachmann 1980).

Identifying slags in the field

Slags at ancient smelting sites can usually be identified in the field. Most ancient slags are ferrous silicates of one type or another (Bachmann 1982). This is usually true regardless of the type of metal (ferrous or non-ferrous) produced at the site. These slags are generally a black or dark gray color. They often exhibit texture due to surface flow, may be layered and striated. Slag can be glassy or crystalline. Slags usually contain pores and/or gas holes, either small or large. Inclusions of various types can be present from unincorporated mineral gangue, charcoal, metal prills, and/or metal sulfides (matte). Slags can contain corrosion products of iron or copper origin, depending on the composition of the original ores. Slags can even have an odor if the original ore was of sulfidic origin. Most slags are heavy, though there are obsidian-like glassy slags that are less dense (Bachmann 1982).

Methodology

Ore Analyses

A selection of ores was surface collected or excavated at El Manchon. In the field, some of these ores were tentatively identified as cuprite, malachite, and arsenopyrite (Jenkins 2001). Pieces of ore that appeared representative of this assemblage were sampled and analyzed using x-ray diffraction in order to determine the crystalline phases present. Four ore samples were analyzed by x-ray diffraction: DH 1.1, DH 1.2, DH 1.3, and DH 3.1. The procedure used is the same as that outlined for the slag analysis (see the section on **Methodology: X-Ray diffraction**). Table 1 shows the x-ray diffraction collection parameters used in the ore analyses.

Table 1. Ore: X-ray diffraction collection parameters.

Sample number	sample type	Filename	run #	divergence slit (deg)	scatter slit (deg)	receiving slit (mm)	sampling interval (deg)	scan speed (deg/min)	step size (deg)
DH 1.1	Ore	Z23618	1	1	1	0.3	5-100	10	0.02
DH 1.2	Ore	Z23969	1	1	1	0.3	10-100	2.5	0.02
DH 3.1	Ore	Z23970	1	1	1	0.15	10-100	2.5	0.02
DH 1.3	Ore	Z23971	1	1	1	0.15	10-100	2.5	0.02

Sidney Carter, a graduate student at MIT's Department of Earth, Atmospheric, and Planetary Sciences (EAPS), prepared thin sections of several ore pieces from El Manchon in August 2001. I analyzed these thin sections by electron microanalysis (see the section on **Methodology: Electron Microprobe**). Dr. Nilanjan Chatterjee of the EAPS department ran the electron microprobe during these determinations.

Field Characterization of Slag

The method

The sample of slags excavated from El Manchon that has been examined in this project was selected from a much larger body of material. In January 2001 Professor Dorothy Hosler and her field team excavated a large slag heap at the site in 6 layers, each measuring 10 cm in depth. For the study reported here, the second layer (10-20 cm deep) was washed and examined. Since one of the goals of this investigation is to produce a manual that archaeologists can use in the field as well as in the laboratory to identify and categorize slag at a metallurgical site, I established a primary group of criteria that would distinguish types or categories of slag on the basis of their gross physical characteristics. Those criteria include slag form (shape), texture, color, sound, and homogeneity (see Table 2). All of these physical characteristics can be determined at a site without the aid of laboratory apparatus.

Process

Initially, the slag was scrutinized without magnification, to search for gross similarities and differences. The **homogeneity** of the slag was one of the first characteristics examined. The amount and type of inclusions (such as crystalline quartz) could indicate how effective the ancient smelting operation was at rendering the entire furnace charge molten. Pieces with many large inclusions were deemed *coarse*. Pieces with a uniform interior (to the naked eye) were termed *smooth*. The **slag form (shape)** was considered: its thickness relative to length and width as well as uniformity of thickness. This led us to

Table 2. Criteria for Slag Categorization.

CRITERIA	CATEGORIES
SLAG FORM (SHAPE)	planar, non-planar, edge, spheroidal
TEXTURE	reticulated, advanced 'grain' growth, cracked/wrinkled, acicular, spongy, corroded, edged/ringed/ridged pores/bumps
COLOR	dark grey, presence of corrosion products (green, pink, or red)
SOUND	clinky (glasslike), non-clinky (dull)
HOMOGENEITY	coarse (crystalline quartz inclusions), smooth (homogeneous appearance)

distinguish between *planar* and *non-planar* types. *Edges* (pieces that have a clearly defined face that solidified against a surface) were separated out for further investigation. The hope is that the edge pieces could potentially be fit together, like a jigsaw puzzle, to yield the shape of the furnace interior within which the slag cooled and solidified (if it was furnace slag rather than tapped slag). Note that the term *edge* can apply to both *planar* and *non-planar* slag types. There were also a small number of slag pieces, usually small in size, that seemed to have no fractured edge and are spherical in shape. These were termed *spheroids;* they have not been treated in this thesis.

After the initial separation into *coarse* and *smooth*, and *planar* and *non-planar* categories, the slags were examined under a low power (x7 – x30) stereomicroscope. In this way, we could identify discrete features on the surfaces of the slag. Since so many pieces of the slag were planar, both sides of the pieces were examined. The **color** and **surface textures** helped refine categories as well. A detailed treatment of the surface textures is given in the section on **Results: Surface Morphologies.**

As the slag pieces were being investigated, we noticed that there were distinctly different **sounds** made when the slag pieces were tapped together or against the examination table. Some of the slag had a very glass-like 'clink' when tapped. Others were decidedly 'dull' sounding. We decided to separate the slag into further categories based on the sound they made. These categories were called *clinky*, for the glass-like sound, and *non-clinky*, for the dull sound.

Laboratory Characterization of Slag

Photography

Many different types of cameras and films were used to capture the images used in this project.

Gross morphologies (photomacrographs)

1. Pictures of small assemblages of slag types were taken with a Nikon FM2 35 mm camera (55 mm macro lens) using Ilford FP4 Plus film.

2. Pictures of experimentally produced heat-modified slags were taken with a Polaroid MP4 Land Camera. The 4" x 5" camera back was loaded with Kodak T-Max film.

Surface features, thin sections, and opaque sections (photomicrographs)

1. Photomicrograph details of slag surface morphologies were taken at a magnification of 8 to 10 times on a Wild Macroskop microscope using both Kodak 4" x 5" T-max film and 4" x 5" Contrast Process Ortho film.

2. Slides of polished cross sections of slag were photographed with incident light on an Olympus polarizing microscope; 35 mm Kodak Ektachrome 64T film was used to capture the images.

3. Slides of ore mineral thin-sections were photographed with an Olympus polarizing microscope, in both transmitted and incident light, at magnifications of 50 – 200; 35 mm Kodak Ektachrome 64 T slide film was used to capture the images.

High resolution photomicrography (SEM)

1. Pictures of the microstructures of the slags were taken with the scanning electron microscope while performing electron microanalysis.

Bulk Chemical Analysis of Slags

Sample selection

Approximately 300 g of each of three categories of slag (smooth planar clinky [DH2Cl.1], smooth planar non-clinky [DH2NC.1], and coarse planar [DH2G.1]) excavated from Level 2 at El Manchon were submitted for bulk chemical analysis. Edge pieces were excluded from this selection because of their importance as individual artifacts in the potential reconstruction of furnace sizes. The samples were sent to Activation Laboratories in Ontario, Canada for analysis. They underwent assay for metallic copper content, ICP-OES analysis for determination of the major oxides and selected trace elements present, and thermal neutron activation analysis for overall trace element content.

Metallic copper assay

The samples were crushed and screened through a mesh. The mesh size for DH2Cl.1 was 100; the mesh size for DH2NC.1 and DH2G.1 was 150. This operation was designed to

flatten the copper prills and larger copper pieces contained in the slag so they would be concentrated on the 'plus side' of the screen (the collection of material which did not pass through the mesh). The weight percentage was then assessed for each sample by weighing the plus and minus fractions (Rittau 2002) (see Section **Results: Bulk Chemical Analysis of Slags**).

ICP-OES whole rock analysis

Samples were prepared using a lithium metaborate-tetraborate fusion and then analyzed using inductively coupled plasma optical emission spectroscopy (ICP-OES). The samples were fused in an induction furnace. While still molten, this mixture was poured into a solution of 5% nitric acid that contained a standard in solution, and mixed for about 30 minutes until it dissolved completely. The samples were analyzed for major oxides and selected trace elements in a combination simultaneous/sequential Thermo Jarrell-Ash ENVIRO II ICP instrument (Rittau 2002) (See Section **Results: Bulk Chemical Analysis of Slags**). Within this instrument, the sample solution is nebulized into a plasma torch. The atoms, once in the plasma, emit light with characteristic wavelengths for each element. An optical spectrometer records the emitted wavelength. The quantity of each element can be determined with standards used to calibrate the instrument (Gill 1997).

Neutron activation analysis

In this analytical method, samples are bombarded by the thermal neutron flux inside a nuclear reactor. Stable isotopes are converted into radioactive isotopes as their nuclei capture neutrons. Once transformed, a radioactive isotope may undergo beta-decay at a known rate and with the emission of a characteristic gamma ray spectrum (Gill 1997). In the case of the El Manchon slags, approximately 30 grams of sample were enclosed in a polyethylene vial and irradiated with flux wires of different elements that provided internal standards. The thermal neutron flux in the reactor was 7×10^{11} n cm^{-2} s^{-1}. The samples were allowed to sit for seven days to allow for the decay of ^{24}Na (Rittau 2002). Sodium is present in high concentration in many samples. Its radioactive isotope, ^{24}Na, with a half-life of 14.97 hours, must be eliminated for the accurate determination of other isotopes that are present. The majority of ^{24}Na decays within the weeklong waiting period (Gill 1997). The samples were then counted with a high purity germanium detector. The resolution of detection with this instrument is better than 1.7 KeV for the 1332 KeV gamma radiation of ^{60}Co. The analyses are checked for accuracy with the flux wires, using a calibration system relying on multiple certified international reference materials. About 10-30% of the samples are checked for accuracy by remeasurement (Rittau 2002).

X-Ray diffraction

The method

X-Ray diffraction was chosen to investigate the types of crystalline phases present within the slag samples recovered from El Manchon. This technique does not determine the

elemental composition of the crystalline material. It uses diffraction data to make a reasonable estimate of the crystalline phases within an unknown sample by comparing the spectra gained from the unknown material with previously investigated spectra of known crystalline materials. Determining the types of crystalline phases in the slags was important to identifying the type(s) of slags present and the smelting operations that may have produced them. In the section **Introduction: Slag**, Bachmann's system of slag categorization is detailed. This system of differentiating slags is structured according to the types of crystalline phases present in a slag. X-ray diffraction is the perfect tool to help identify such phases.

X-rays are dispersed in different directions upon interaction with a crystal according to the wavelength of the x-radiation. The diffraction of x-rays in crystals can be described by the Bragg equation:

$n\lambda = 2d\sin\theta$

θ = angle of incidence
λ = wavelength
n = the order of the reflection
d = interplanar spacing between crystal lattice planes

When a collimated x-ray beam of wavelength λ is incident at an angle θ on a crystal with crystal planes of spacing d, a reinforced, coherent scatter of the radiation occurs at the angle of reflection θ when Bragg's law is satisfied for an integer number n (Ciliberto and Spoto 2000).

The incident x-rays that are scattered according to the above equation are diffracted, due to constructive interference, in a beam at the same theta value as the angle of incidence.

In x-ray spectrometry, a large single crystal cut parallel to a known set of planes is used to separate an x-ray beam diffracted from an unknown material into its component wavelengths. The wavelengths can be calculated because the angle of incidence is known. Additional amorphous phases are not detected using this technique (Gill 1997).

The computer program used in these analyses calculates probabilities that known crystalline materials are matches for the unknowns. The challenge lies in the fact that the samples being analyzed are not necessarily composed of a single, pure material. The output of an x-ray diffraction analysis is given in the form of a spectrum that contains high-intensity peaks that appear at diffraction angles (2θ) where the Bragg equation is satisfied. The crystallographic planes that satisfy the equation are known. The spectrum of an unknown material is compared to known spectra, and the operator can determine the most likely match based on other auxiliary data, such as elemental analyses previously determined for the unknown (Callister 2000).

Sample preparation

X-Ray diffraction analysis was performed on both ore samples and slag samples from El Manchon. A small amount of sample (27 mm^3) was ground to a fine powder (the consistency of talcum powder, where possible) in a diamonite mortar and pestle. Powdering of the sample is done to ensure that all possible sets of crystallographic planes are available for diffraction. Diamonite, a very hard, synthetic material, was used in lieu of an aluminum oxide mortar and pestle to prevent contamination of the sample from the mortar and pestle material. Between each sample, the mortar and pestle were cleaned by

grinding pure quartz sand (SiO_2) several times and scouring with Ajax abrasive cleaner. To ensure that no cross-sample contamination occurred, the mortar and pestle were examined under a microscope at low magnification to confirm visually the elimination of traces of the previous sample.

The finely ground slag samples were adhered to glass slides. A clear gel of collodium (a nitrocellulose and ether solution) was mixed with the powdered sample in a crucible and spread onto a glass slide with a spatula. The slide was subsequently air dried for approximately 30 minutes. This procedure was necessary, because the slag samples typically contained phases that were too hard to be ground to the appropriate degree of fineness. Thus the slag sample particles were not completely uniform in size. The ore samples, which were far easier to grind to the appropriate fineness, were simply 'packed' into a shallow basin on an XRD sample slide.

Four ores samples and three slag samples were analyzed (see Table 3). The ore samples are reported in **Results: Ore Analyses**. The samples were analyzed using a Rigaku RTP 500 RC 250 mm high-resolution diffractometer with the assistance of Mr. Joseph Adario. The samples were run on three different days and at slightly varying parameters. The sampling interval and/or scan speed was modified in some cases to confirm or deny the presence of a particular peak or set of peaks. The data were analyzed using the Jade 6 computer program to assess the probabilities of particular phases being present in the samples. A low scan speed allows a clearer plot of the diffracted wavelength peaks. Some

scans were performed over a very small sampling interval to define more clearly a previously identified feature.

Table 3. Slag: X-ray diffraction collection parameters.

Sample number	Sample Type	filename	run #	divergence slit (deg)	scatter slit (deg)	receiving slit (mm)	sampling interval (deg)	scan speed (deg/min)	step size (deg)
DH2.17	Non-Clinky	Z23623	1	1	1	0.3	10-100	10	0.02
DH2.17	"	Z23694	2	1	1	0.3	10-100	10	0.02
DH2.17	"	Z23697	2	1	1	0.3	20-75	2	0.02
DH 2.18	Coarse	Z23621	1	1	1	0.3	10-100	10	0.02
DH 2.18	"	Z23622	2	1	1	0.3	10-100	3	0.02
DH2.19	Clinky	Z23619	1	1	1	0.3	10-100	10	0.02
DH2.19	"	Z23620	2	1	1	0.3	30-100	2	0.02
DH2.19	"	Z23695	3	1	1	0.15	31-32	0.5	0.01
DH2.19	"	Z23696	3	1	1	0.15	50.5-52.5	0.5	0.01

Electron Microprobe

The method

Electron microprobe analysis allows the researcher to analyze an area of a few square microns on the surface of a sample. A beam of electrons is finely focused to probe a semi-spherical volume of only a few microns in diameter. The characteristic x-rays that are emitted upon interaction with the electron beam identify the elements present in a sample. The intensity of a particular wavelength compared to a standard of the same element allows the user to quantify the abundance of that element in the sample. The beam is focused on an area of the sample by locating the feature on a scanning electron microscope (SEM) image of the surface of the sample (Chatterjee 2001).

Two kinds of information are gathered by the electron microprobe. An energy-dispersive spectrum (EDS) allows the user to identify qualitatively the particular elements in the

sample located at the position of the electron beam. A wavelength-dispersive spectrum (WDS) is then determined in order to obtain a quantitative analysis only of those elements chosen for analysis. This cuts down on the amount of time spent per sample, as only the elements of relevance are analyzed using the more sensitive technique.

The phase of the materials located at the point of analysis can be extrapolated by examining the atomic ratios of the elements present there. Eventually, by correlating the SEM images with known phase compositions, inferences can be drawn about the formation of multi-phase structures within the samples (Gill 1997).

Sample preparation

A fine polish on the surface of the sample is required for quantitative microprobe analyses. The slag sample to be polished was sliced from a large piece using a gem saw. The sample was dried and mounted in bakelite or epoxy. A silicon carbide strip grinder with 240, 320, 400, and 600 grits and water lubrication was used for the initial grinding of the sample. Grinding the mounted slag against the grit generated parallel striations. The sample was rotated through ninety degrees between successive grits to eliminate all traces of the previous striations. The surface was examined under magnification to ensure that all lines from the previous grinding were eliminated.

After initial grinding, the sample was polished on a rotating wheel first with 6-micron diamond paste and then with 1-micron diameter diamond paste. Again, the surface of the

sample was examined under a microscope to ensure all traces of the previous level of polishing had been eliminated. Finally, the surface was swabbed with cotton wool dampened with a soapy lather in deionized water. The samples were then stored in a desiccator to prevent surface oxidation.

Since the slag and ore specimens are non-conducting, they had to be coated with a thin film of carbon (approximately 20 nm thick) before being introduced to the sample chamber. This is done to avoid the accumulation of charge on the surface of the sample (Gill 1997). The coating is grounded to the metal specimen holder using a line of colloidal graphite paint.

One ore sample and seven slag samples were analyzed **(See section Results: Electron Microprobe** and **Results: Ores)**. The samples were analyzed using a JEOL JXA-773 Superprobe with a 15 KeV voltage and a 10.003 or 10.009 nA current. Dr. Nilanjan Chatterjee of MIT's Department of Earth, Atmospheric and Planetary Science operates this instrument. Scanning electron microscope images were taken of the surface regions analyzed with the electron microprobe.

Thermal experiments

The method

Determining the temperature at which a smelting operation occurred is key to evaluating the level of sophistication of the technology practiced by the metalworker. One way to approximate internal furnace temperature is to determine the temperature at which the slag slumps or becomes molten and runs. We used a muffle furnace to raise the

temperature of excavated pieces of slag, observing them in the furnace through an observation port as furnace temperature was increased. This allowed us to determine the temperature range over which the slags altered shape, from solid, angular pieces to smooth, slumped, and partially molten materials. This technique was chosen because it most closely approximates (within our capabilities) the thermal environment in which the slags may have been formed in antiquity.

Sample preparation

A medium-sized piece of slag (approximately 15mm x 10mm x 5mm) was inserted into an alundum boat and placed into a furnace preheated through manual controls to 800°C. Nitrogen was introduced into the furnace at ambient temperature and flowed continuously during the experiment. This prevented the slag from oxidizing excessively. Above 800°C the temperature inside the furnace was increased at a rate of 6°C/minute using a ramping program. Two thermocouples monitored temperature. One thermocouple was suspended very close to the piece of slag and above the alundum boat; the other was located at the back of the furnace, near the chamber roof. The maximum temperatures achieved in these experiments ranged from 1100°C to 1278°C. We varied the maximum temperatures to try to produce different surface morphologies on the slag samples so that we could compare them with the excavated slags. Maximum temperatures also varied according to our visual estimate of the onset of melting.

A few of the first experiments were carried out in a Blue M Box Type Muffle Furnace in an air atmosphere, but the furnace temperature could not be raised above 1100°C. Most of the experiments were done in a CM Inc. Rapid Temperature Furnace (muffle). Dr.

Harold Larson guided us in the proper operation of the furnace setup, and Professor Heather Lechtman and I ran the experiments together. Two types of temperature readings were recorded; the 'set point' and the furnace temperature. The set point temperature was that which was given by the thermocouple at the rear of the furnace. The furnace temperature was the temperature given by the thermocouple located at the slag sample. There was often a difference of approximately 50°C in these readings. We used the furnace temperature values to indicate the temperature to which the slag was raised.

Observations of the slag pieces through a viewing port in the furnace door were possible at temperatures up to about 950°C. At the higher temperatures the slag was so hot that its color could not be distinguished from that of the white-hot furnace walls; it became almost undetectable without the use of dark goggles. In most cases the alundum boat was removed when the slag showed signs of slumping, and the slag cooled in air. The resultant heat-modified slag pieces were examined under low power magnification and photographed.

Results

Ore Analyses

Physical Description of Ores

A physical description made prior to analysis of the ore samples is given in Table 4. Figure 8 shows an assemblage of some ores recovered from El Manchon.

Table 4. Description of ore samples analyzed.

Sample Number	Excavation Location	Description
DH 1.1	Level 1 (0-10 cm)	bright green ore
DH 1.2	Level 1 (0-10 cm)	ore with three distinct visual sections: green, reddish, and transparent
DH 1.3	Level 1 (0-10 cm)	dark color, possibly specular hematite (geologist's ID)
DH 3.1	Level 3 (20-30 cm)	dark, reddish

X-Ray diffraction

The four ore samples described in Table 4 were analyzed by x-ray diffraction. The collection parameters used for these samples are reported in **Methodology: Ore.** In sample DH 1.1, the standard spectrum for malachite shows a strong match (Fig. 9). In sample DH 1.2, malachite and quartz are present (Fig. 10). The sample DH 1.3 was a challenge to decipher. Cuprite, wüstite, and quartz were all plausible potential matches for the sample. Most likely the sample is a conglomerate of all of these phases. We feel that the best matches identify cuprite and wüstite (Fig. 11). The sample DH 1.3 shows matches for quartz and hematite (Fig. 12).

Photography of Ore Thin Sections

Thin sections of ores were scrutinized with a petrographic microscope and viewed under cross-polarization. The ore shown in Figure 8 is composed of mostly green, brown and white mineral and rock domains (see Fig. 13). XRD analyses of similar samples identified the green as malachite, the brown as iron oxide, and the white as quartz rock. In addition, towards the interior of two of the ore samples (see Figs. 14 and 15), there are gold and gray opaque mineral domains.

The map in Figure 16 records the location of the photomicrographs shown in Figures 13, 14, and 15 taken of the cross section of ore 4-13 (see Table 5). The γ region (shown in Fig. 13) is closer to the surface of the ore than the α and β regions shown in Figures 14 and 15, respectively. This led us to suspect that the opaque minerals closer to the interior of the samples are remnants of the types of minerals to be found in the primary ore body of the deposit that the ancient metalworkers of El Manchon were mining. The oxidation process altered the outer layers of this sample of ore, judging by the distribution of its minerals.

Electron Microprobe Analysis

Through electron microprobe analysis, the gold and gray domains of ore samples 4-13 and 4-15 were identified as pyrite, an iron sulfide (FeS_2). Table 5 presents the data obtained from these analyses given as weight percents of the elements. The concentrations of iron, copper, and sulfur were determined within the gold and gray

domains. No copper was detected at any of the points analyzed. The pyrite is present as a vestige of the original, primary, and unweathered sulfide ore.

Table 5. Electron microanalysis of sulfide domains in ore thin section.

Sample #	Trial	Composition wt%		
		Fe	S	Total
Ore 4-13	1	43.65	56.05	99.7
	2	45.03	55.72	100.75
	3	43.93	55.64	99.57
Ore 4-15	1	45.72	55.63	101.35
	2	44.49	55.3	99.79
	3	45.84	55.06	100.9
Mean Composition		44.77	55.57	100.34

Slag Types

Two sets of major types of slags arose from the characterization process (see **Methodology: Characterization of Slags**): *smooth* slag and *coarse* slag and, within the smooth designation, *clinky* and *non-clinky*. Smooth slags are characterized by: slight internal variation based on observation of broken sections with the naked eye, a large surface area relative to thickness (large, thin, flat pieces), and surface morphologies that can be separated into various categories. Within the *smooth* designation, the slag can be further differentiated into clinky and non-clinky slags. The only noticeable difference between these two types is the sound that they produce when tapped against a hard object. *Clinky* slag makes a sound akin to that of glass. *Non-clinky* slag makes a dull tapping sound distinctly unlike the 'clink.' Figures 17 and 18 illustrate smooth-clinky and smooth-non-clinky slags.

Evidence of the various surface morphologies is apparent in Fig. 17; these are considered in detail in the section on **Results: Surface Morphologies**. All smooth slags can be classified as planar, given that none of the smooth slags examined was irregular in thickness.

The interiors of coarse slags as seen in broken section are characterized by a high incidence of inclusions, such as bits of crystalline quartz. This material is most likely unmelted gangue that was not removed from the metallic mineral after mining. In addition, the thickness of the coarse slags is not necessarily uniform across an entire sample; the slag can be planar (uniform thickness) or non-planar (irregular thickness). Figure 19 shows a variety of coarse slags. No regularity in surface morphologies was observed on the coarse slag pieces. Occasionally part of a surface morphology similar to those observed on the smooth slag pieces might be detected on the coarse slag surface, but without the consistency necessary to lead to further categories within the coarse slag type.

Surface Morphologies

A number of morphological features were observed on the exterior of the slags categorized as smooth and planar. Both the non-clinky and clinky varieties of these slags exhibt these surface morphologies. In only one case is a particular morphology much more common in the clinky as opposed to non-clinky slags. The wrinkled/cracked surface

(see Figure 20) seems to be far more common in the clinky variety of smooth-planar slags. In the other categories, no preference has yet been detected. The following surface features have been documented: edged, ridged, or ringed pores and bumps; acicular; spongy; corroded; wrinkled/cracked; reticulated; advanced 'grain' growth; pink, ridged, streaked.

Wrinkled/cracked surface (Figure 20)

This surface appears to be a thin, wrinkled, and/or cracked membrane that floated atop a region of less perturbed slag. The surface is fairly smooth aside from the wrinkles and cracks. Occasionally, a piece might also have pores or bumps. Approximately 1 in 4 of these pieces is an edge piece. Edge pieces have a characteristic side that appears to have solidified against a surface, forming a lip. Presumably, this feature was caused by slags that abutted the interior furnace lining as they cooled and solidified. The observed wrinkles tend to be spaced equally and are parallel. The less parallel the wrinkles are, the shorter they tend to be.

Reticulated surface (Figure 21)

The reticulated surface is a network of uniform raised or depressed, nearly circular units. Two main types are observed: (1) a network of ridges around nearly circular depressions [bubble impressions]; (2) a network of raised bumps that occur in varying densities across the surface. The reticulated surface is extremely common and is observed on one

side of most of the smooth, planar slag pieces. It is uncommon to see this feature on both sides of a planar slag piece, however.

Spongy surface (Figure 22)

Amorphous sunken domains within a smooth featureless matrix characterize the pattern on this surface. The pattern is similar to the impression left when painting with a sponge. This type might potentially be related to the acicular type, but it clearly lacks the well-developed elongated crystals that characterize acicular surfaces.

Corroded surface (Figure 23)

This surface exhibits a high concentration of metal corrosion products. The characteristic green copper carbonates and chlorides and red iron oxides are common on surfaces of this type. This surface tends also to be covered with pores and voids, some of which, being filled with metal corrosion, might have once held copper prills trapped in the slag.

Advanced 'grain' growth surface (Figure 24)

This surface is characterized by large (~1-2mm), squarish grains that have grown and solidified on it. An individual grain is often surrounded by a 'sunburst' pattern reminiscent of the feathery growths emanating from the sides of the crystals on acicular surfaces. Sometimes a grain exhibits a pyramidal form and appears to have grown

perpendicular to the surface. Surfaces of this type are sometimes covered with a thin, pinkish film (corrosion products?).

Pink ridged, streaked surface (Figure 25)

This surface has an overall pink cast and is sometimes streaked silvery gray. There are ridges of varying size on the surface and occasional areas of frothy, bubble-covered slag.

Ridged, ringed pores and bumpy surface (Figure 26)

This surface can have any combination of the following: ridged pores (pores with a raised rim around them, almost crater-like), ringed pores (the ring is not raised), and bumps. Metallic corrosion products sometimes accompany this surface.

Acicular surface (Figure 27)

This surface is characterized by needle-like crystal growths. At high magnification there appear to be feathery growths surrounding the crystals, jutting out perpendicular to their surfaces. There appear to be various stages of crystal growth. The crystal morphology can range from scattered paths of a few crystals to a three-dimensional mass of crystals that appears to be 'growing out' of the surface of the slag.

Bulk Chemical Analysis of Slags

Three slag categories were analyzed for their bulk metal and oxide compositions and for trace element determinations. The methods used were metallic assay for copper, ICP-OES Whole Rock analysis, and neutron activation analysis. For information on sampling, see the section **Methodology: Bulk Chemical Analysis of Slags**.

Metallic Copper Assay

Table 6 shows the weight percentages of copper still present in the slags, as determined by a metallic copper assay. The procedure is described in the section **Methodology: Bulk Chemical Analysis of Slags**.

Table 6. Metallic copper determination for slags (wt %).

Sample	Type	Cu% -	Cu%+
DH2CL.1	clinky	1.641	1.584
DH2NC.1	non-clinky	1.398	1.03
DH2G.1	coarse	2.144	1.511

ICP-OES Whole Rock Analysis

The weight percentages of certain oxides were determined for the different slag types. Table 7 shows the results of these determinations.

Table 7. Oxide determination for slags.

Sample	Type	Oxide Percentages, by weight											
		SiO_2	Al_2O_3	Fe_2O_3	MnO	MgO	CaO	Na_2O	K_2O	TiO_2	P_2O_5	LOI[1]	Total
DH2CL.1	Clinky	38.7	4.33	56.62	0.07	0.5	1.05	0.1	0.3	0.2	0.29	-5.32	96.805
DH2NC.1	Non-clinky	39.6	4.69	56.29	0.07	0.5	1.07	0.21	0.4	0.2	0.28	-5.28	98.029
DH2G.1	coarse	57.7	3.61	37.08	0.07	0.5	1.07	0.08	0.4	0.2	0.23	-3.21	97.76

[1] LOI = Percent Loss on Ignition

An additional analysis was performed to determine the relative quantities of FeO and Fe_2O_3 in the slags. The first analysis tested only for Fe_2O_3 (Table 7). The relative quantities of the iron oxides were required for the selection of an appropriate ternary phase diagram to model the system (See **Results: Thermal Experiments**). The results of the second analysis are shown in Table 8.

Table 8. Iron oxide concentrations (weight %).

Sample	Type	FeO	Fe_2O_3
DH2CL.1	Clinky	3.823	48.28
DH2NC.1	Nonclinky	6.818	44.19
DH2G.1	coarse	4.738	28.66

ICP Trace Element Analysis

An ICP analysis was carried out to provide a quantitative determination of the trace elements present in the slags; the results are shown in Table 9.

Table 9. ICP trace element analysis.

Sample	Type	Ag ppm	Cd ppm	Ni ppm	Pb ppm	Zn ppm	Bi ppm	S %	Ba ppm	Sr ppm	Y ppm	Sc ppm	Zr ppm	Be ppm	V ppm
DH2CL.1	Clinky	2.8	-0.3	18	190	470	7	0.1	1816	104	34	5	54	1	101
DH2NC.1	Nonclinky	2.9	-0.3	15	217	768	-2	0.2	3772	105	36	8	62	1	125
DH2G.1	coarse	10.3	0.4	15	79	385	6	0.3	2106	78	36	4	56	-1	88

Neutron Activation Analysis

A neutron activation analysis determination of the trace elements present in the slags was performed as a complement to the ICP analysis; the results are shown in Table 10.

Table 10. Neutron activation trace element analysis.

Sample	Type	Ir ppb	Mo ppm	Rb ppm	Sb ppm	Sc ppm	Se ppm	Ta ppm	Th ppm	U ppm	W ppm	Zn ppm	La ppm	Ce ppm
DH2CL.1	Clinky	-5	160	50	37	6.5	-3	-0.5	3.2	11.3	169	656	30	40
DH2NC.1	Nonclinky	-5	160	-15	54	6.3	-3	-0.5	3	11	154	997	34	49
DH2G.1	coarse	-5	95	-15	70	4.5	-3	-0.5	2.4	7.2	110	535	25	36
		Nd ppm	Sm ppm	Eu ppm	Tb ppm	Yb ppm	Lu ppm	Au ppb	As ppm	Br ppm	Co ppm	Cs ppm	Hf ppm	
DH2CL.1	Clinky	17	5.5	1.3	1	3.4	0.5	19	49	-0.5	517	55	-1	
DH2NC.1	Nonclinky	28	6	1.3	1.2	4	0.6	50	64.6	-0.5	570	58	-1	
DH2G.1	coarse	13	4.8	1	0.7	3.5	0.5	452	243	-0.5	355	46	-1	

X-Ray Diffraction Analysis of Slags

Three slag samples were analyzed with the x-ray diffractometer. The sample DH 2.19 is a smooth, planar, and non-clinky type. The sample DH 2.18 is a coarse, planar type. The sample DH 2.17 is a smooth, planar, and clinky type. For the collection parameters used for these samples, see **Methodology: X-Ray Diffraction.**

The spectrum generated by sample DH 2.19 shows a strong match with the standard spectrum for fayalite (See Fig. 28) and a possible, much weaker match with chalcocite (Cu_2S). In sample DH 2.18, cristobalite (a polymorph of SiO_2) is present as well as fayalite, quartz, and copper (see Fig. 29). The sample DH 2.17 shows a match with fayalite (See Fig. 30) and with metallic copper.

All three of the slags show the strong presence of crystalline fayalite. This is corroborated by images of fayalite crystals taken with the scanning electron microscope as well as by

electron microprobe analyses of these crystalline phases. See the section **Results: Electron Microprobe** for these data.

Electron Microprobe

Slag samples analyzed

The data reported in this section result from wavelength-dispersive spectrometric (WDS) analysis of slags, as described in the section **Methodology: Electron Microprobe**. The data are organized in two different ways to facilitate interpretation. First, a SEM image of the analyzed area of each sample is shown. In the second section, the data are organized according to the category of the microstructural feature analyzed.

The slags examined, in general, were primarily crystalline phases embedded in glassy matrix phases. They contain prills of metal that are copper-red in color and phases, distributed both within the prills and throughout the matrix material, that appear to be sulfide mattes. Table 11 lists the type of each slag sample analyzed as well as the number of points analyzed in each category. At features labeled "copper prills" or "sulfur matte," the elements Cu, S, and Fe were analyzed, since prior qualitative EDS scans indicated their presence. Programs used in the analysis of the crystalline (olivine.qnt) and glassy (glass.qnt) phases were provided by Dr. Nilanjan Chatterjee.

Table 11. Samples analyzed with electron microprobe and type of microstructures investigated.

Sample #	Slag Category	Number of Points Analyzed Using WDS			
		Cu prill	S matte	crystalline	glassy
MIT 5258-A	coarse	2	3	2	1
DH 2.1-1	smooth, planar, clinky	1	2	1	1
DH 2.13-1	smooth, planar, non-clinky	1	1	1	1
DH 2.12-1	coarse, planar	0	0	1	1
DH 2.5-1	smooth, planar, clinky	0	0	0	1
DH 2.14-1	coarse, planar	0	0	0	2
DH 2.15-1	smooth, planar, non-clinky	1	1	1	1

Scanning Electron Microscope Images of Slag Interiors

For every slag sample analyzed by electron microscopy, a list is provided of the points analyzed, and the location of the points is specified on a SEM image, where available. "Matrix" denotes a glassy region that is close to and surrounds a crystalline phase. A "matte inclusion in prill" refers to small regions of matte that are contained within the body of a copper prill. Sometimes a shade (dark, light) is referred to. This is intended to be a description of the comparative shades in a sample, not an absolute color definition.

MIT 5258–A: 8 points analyzed (Fig. 31)

1. copper prill
2. copper prill
3. massive matte
4. massive matte
5. matte inclusions in prill
6. crystalline slag
7. crystalline slag
8. glassy slag

DH 2.1–1: 5 points analyzed (Fig. 32)

a. matte
b. matte inclusions in prill
c. copper prill
d. crystalline slag needle
e. glassy matrix

DH 2.13–1: 4 points analyzed (Figs. 33 and 34)

a. light-colored crystal
b. dark glassy matrix
c. copper prill (no photo available)
d. matte (no photo available)

DH 2.12 –1: 2 points analyzed (Fig. 35)

a. large gray crystal
b. quenched margin-like dendrites (no analysis made)[2]
c. white prill within gray crystal

DH 2.5–1: 1 point analyzed (Fig 36)

1. glassy pocket

DH 2.14–1: 2 points analyzed (Figs. 37 and 38)

1. light-colored glassy
2. dark-colored glassy

DH 2.15–1: 4 points analyzed (Figs. 39 and 40)

1. copper prill
2. matte (near prill)
3. roughly square crystals
4. dark, glassy matrix

[2] 'margin-like' refers to the fact that there are crystals aligned along the edge of the larger gray crystal and can be described as a margin between the gray crystal and the region of more typical elongated fayalite crystals in amorphous fayalite matrix.

Quantitative WDS Results, Reported by Type of Feature Analyzed

Copper prill:

Table 12. Composition of copper prills.

sample #	type of point	#	Composition (El-Wt%)			
			Cu	Fe	S	Total
MIT 5258-A	prill	1	97.38	0.4728	0.0008	97.85
MIT 5258-A	prill	2	97.49	0.4064	0.0004	97.89
DH 2.1-1	prill	c	99.5	1.9385	0.0161	101.46
DH 2.13-1	prill	c	99.53	0.5979	0.0053	100.14
DH 2.15-1	prill	1	101.76	1.1959	0.0058	102.96

From the data in Table 12, it is clear that the metal produced during smelting was almost pure copper.

Sulfide matte:

Table 13. Composition of matte.

sample #	type of point	#	Composition (El-Wt%)			
			Cu	Fe	S	Total
MIT 5258-A	Matte	3	66.96	7.98	24.32	99.26
MIT 5258-A	Matte	4	77.26	1.1284	21	99.39
MIT 5258-A	matte inclusion in prill	5	78.15	1.1798	21.38	100.71
DH 2.1-1	Matte	a	78.41	1.0878	20.97	100.46
DH 2.1-1	matte inclusion in prill	b	79.12	1.7739	21.12	102.01
DH 2.13-1	Matte	d	78.41	1.5359	20.88	100.82
DH 2.15-1	Matte	2	78.88	2.23	20.26	101.36

The presence of sulfide matte in the slag matrix material and in the copper prills indicates that the furnace charge contained some sulfur, most likely in the form of sulfide ore. As the section **Results: Ore Analyses** indicates, tiny patches of primary sulfide mineral (pyrite) remain in the weathered copper ore charged into the smelting furnaces. However, we do not think that the smelting process at El Manchon deliberately used sulfidic ores

because the volume fraction of matte in the slags is so low. By comparison, in smelting operations that include sulfide ores in the charge, the matte phase separates from the slag and is then visible to the naked eye (Lechtman and Klein 1999). From the atomic percent data generated during the electron microanalysis of the matte we calculated that the composition of the sulfide matte is close to that of chalcocite (Cu_2S), with some component of iron, possibly as FeS_2.

Crystalline slag:

Table 14. Composition of crystalline phase (expressed as oxides).

			Composition (Oxide-Wt%)									
sample #	phase/feature	#	SiO_2	TiO_2	Al_2O_3	Cr_2O_3	FeO	MnO	MgO	CaO	NiO	Total
MIT 5258-A	crystalline	6	30.04	0.02	0.198	0.0314	66.13	0.1363	2.0172	0.0999	0.0296	98.7
MIT 5258-A	crystalline	7	35.48	0.043	1.9977	0.0036	58.11	0.1282	1.1468	0.3846	0	97.29
DH 2.1-1	needle	d	34.21	0.05	0.6722	0	63.64	0.1593	0.8344	0.1197	0.0172	99.7
DH 2.13-1	crystal	a	40.29	0.358	4.27	0	50.11	0.0313	0.2279	0.4769	0	95.76
DH 2.12-1	crystal	a	28.86	0.025	0.1974	0.012	69.19	0.2011	0.5711	0.5519	0.0332	99.64
DH 2.12-1	crystal	c	35.07	0.707	0.7074	0.012	61.03	0.1076	1.278	0.1537	0.0134	98.37
DH 2.15-1	crystal	3	51.09	0.533	12.09	30.69	0.091	0.0677	2.94	0.4096	0.5951	98.8

The primary mineral in the crystalline slag is fayalite ($2FeO{\cdot}SiO_2$). A phase analyzed in sample DH 2.15-1 exhibits a composition vastly different from the majority of the crystalline areas in the slag. The aluminum oxide component is 12.09%, highly elevated above the minor contents of Al_2O_3 in most other slags, and the SiO_2 content is about 1.5 times higher than the average slag silica values. In addition, the morphology of the crystals (Fig. 40) is unusual; the grains are square and appear to be twinned (growing out of one another). Plotting the values for this phase composition on the $FeO\text{-}SiO_2\text{-}Al_2O_3$ ternary phase diagram indicates that the phase is tridymite (SiO_2) rather than fayalite. The unique morphology evident in the SEM photo in Figure 40 corroborates this finding:

tridymite exhibits a characteristic "triplet" twinning in which the crystals appear to be growing out of each other in rays (Rudolph 2000).

Glassy slag:

Table 15. Primary element composition of glassy phase (expressed as oxides).

			Composition (Oxide-Wt%)									
sample #	phase/feature	#	SiO_2	TiO_2	Al_2O_3	FeO	MnO	MgO	CaO	K_2O	P_2O_5	Total
MIT 5258-A	glassy	8	52.53	0.3725	11.28	24.75	.0449	0.1617	2.4979	0.8121	0.4741	93.11
DH 2.1-1	matrix	e	49.24	0.8129	12.54	0	31.21	0.1414	0.1170	2.0492	0	96.10
DH 2.13-1	glassy matrix	b	44.88	0	6.76	0	40.88	0.1648	1.1437	3.30	0	97.13
DH 2.15-1	glassy	4	42.87	0.4097	5.91	48.01	0.0697	0.0440	0.5312	0.5071	0.1731	98.69
DH 2.5-1	glassy pocket	1	53.65	0.4497	13.01	26.54	0.1101	0.0595	3.84	0.3283	0.5071	98.70
DH 2.14-1	light glassy	1	48.44	1.0655	16.86	29.83	0.0864	0.3790	2.0331	0.8841	0.1160	99.85
DH 2.14-1	dark glassy	2	46.79	0.3697	8.33	34.34	0.0816	0.0261	7.60	1.2268	0.1827	99.97

Most of the elements determined in the slags were investigated using a program specifically for the analysis of glasses (glass.qnt). The regions identified as glassy phases (see Table 15) have a higher concentration of SiO_2 compared to the crystalline phases (see Table 14). In addition, the concentration of FeO is significantly lower in the glassy regions. There is also a higher incidence of CaO and Al_2O_3 within the glassy phases. The levels of compounds including Cr_2O_3, MnO, MgO, and NiO (see Tables 15 and 16) appear to vary little between the glassy and crystalline phases. K_2O, P_2O_5, S, and Na_2O were not measured in the crystalline phases, thus their values cannot be compared with the glassy phase.

Table 16. Secondary element composition of glassy phase.

sample #	phase/feature	#	Composition (Oxide-Wt%)				
			Cr_2O_3	Na_2O	NiO	S	Cl
MIT 5258-A	glassy	8	0	0.0927	0.013	0.081	0
DH 2.1-1	matrix	e	0	-	0	-	-
DH 2.13-1	glassy matrix	b	0	-	0	-	-
DH 2.15-1	glassy	4	0	0.7043	0.079	0	0.016
DH 2.5-1	glassy pocket	1	0	0.1409	0.030	0.019	0.021
DH 2.14-1	light glassy	1	0	0.1358	0.051	0.183	0
DH 2.14-1	dark glassy	2	0	0.0906	0.072	0.808	0.052

Thermal History of the El Manchon Slags

Melting Temperature Calculations

The bulk compositional analyses of the slags (see Tables 7-10) were used to calculate their equilibrium melting temperatures by plotting the results on a SiO_2-Al_2O_3-FeO ternary phase diagram (Fig. 41). Because of their relative uniformity, melting temperatures were determined only for the smooth clinky and the smooth non-clinky slags. No determination was attempted for the coarse slags because they contained many unmelted, crystalline, rocky domains. The large difference in melting temperatures between these domains could not be accommodated by this method.

Figures 41 and 42 locate the melting points of the smooth clinky and smooth non-clinky slags on the SiO_2-Al_2O_3-FeO equilibrium diagram. Isotherms of different melting temperatures within the phase fields provide the most likely range of slag melting temperatures. When making the plots, we added to the FeO analysis the concentrations of a group of oxides that act similarly to FeO in materials such as these slags: MnO, MgO,

CaO, Na_2O, and K_2O. The Fe_2O_3 values were also converted into FeO. The P_2O_5 and TiO_2 values were not included in the sums.

The weight percentages of the FeO-type oxides given by the bulk analyses were converted to mole percentages, added together, and then converted back to weight percent to provide the value used for FeO. By adding all these components to the FeO value a narrower distribution of potential melting temperatures was obtained. Ideally, the three major components ought to sum to 100% so that a point can be plotted accurately on the ternary phase diagram. This was not possible given the composition of the slags, which included small amounts of many additional elements (see Tables 7 – 10). Slags are, after all, collectors of impurities.

In Figures 41 and 42 the triangles corresponding to the bulk composition of these slags overlap the fayalite and tridymite phase fields on the ternary diagram. The melting temperatures of these slags range from 1150°C to 1200°C. We submitted our bulk chemical analysis data to Dr. Henri Gaye (Department of Physical Chemistry, IRSID, Maizières-lès-Metz, France). He used a complex computer program to determine the melting temperatures for the smooth slags (Lehmann et al. 1990). He estimates the liquidus temperatures to be approximately 1150 to 1160°C (H. Gaye, personal communication, 2002).

Furnace Experiments

In order to measure experimentally the temperatures at which the slags slumped and/or melted, we conducted thermal tests on pieces of excavated slags using the heat treatment facilities of the DMSE Welding Laboratory. A Blue M Box Type Muffle Furnace with a range of 0 - 1100°C and a CM Inc. Rapid Temperature Furnace (muffle) that operates at considerably higher temperatures were used to heat the slags. The Blue M furnace is outfitted with a thermocouple at the rear of the furnace chamber, not at the sample location. The CM Inc. furnace has one thermocouple located at the rear roof of the chamber. We placed a second thermocouple close to the sample and monitored it with a direct reading, external Type K chromel-alumel Fluke 54 II Recording Potentiometer. We were able to record sample temperatures at the slag position. The CM furnace has a viewing port that allowed us to record the change in shape of the slag as it slumped at the higher temperatures.

The samples, contained in alundum refractory boats, were introduced into the furnaces once they had been preheated to approximately 800°C. In the case of the CM furnace, a ramping program then raised the furnace temperature at the rate of approximately 6°C per minute. The slags treated in the Blue M furnace were heated in air; the chamber of the CM furnace was filled with nitrogen during the preheat period, and the nitrogen continued to flow during the course of the experiment. Table 17 gives the operating conditions of each set of thermal experiments. Figure 43 illustrates a few of the experimentally heated slags.

Table 17. Operating conditions of thermal experiments.

						Soak	
Sample #	Run #	Type	Atmosphere	Furnace	Maximum T (°C)	Time (min)	Temperature (°C)
DH 2.14	1	coarse	air	Blue M	1100	15	1100
DH 2.13	1	non-clinky	air	Blue M	1100	15	1100
DH 2.4	1	clinky	air	Blue M	1100	15	1100
DH 2.4	2	clinky	air	CM Inc.	1200	none	
DH 2.13	2	non-clinky	N2	CM Inc.	1200	none	
DH 2.14	2a	coarse	N2	CM Inc.	1200	none	
DH 2.14	2b	coarse	N2	CM Inc.	1280	7	1280
DH 2.17	3	clinky	N2	CM Inc.	1100	10	1100
DH 2.19	3	non-clinky	N2	CM Inc.	1150	10	1150
DH 2.18	3	coarse	N2	CM Inc.	1200	10	1200

Slag samples DH 2.14-1, DH 2.13-1, and DH 2.4-1, all heated in air to 1100°C, showed very little change in gross morphology, save for changes in the microscopically visible surface morphologies. For example, DH 2.13 –1 developed a surface (Fig. 44) much like the reticulation exhibited by many of the El Manchon slags and illustrated (Fig. 21) in the **Surface Morphologies** section. No slumping was observed in any of these samples heated to 1100°C. DH 2.4 – 1 appears to have lost some of its clinky properties as a result of heat treatment. The pitch of the sound produced when the heated sample is tapped against a hard surface is different from the sound it made originally and that classified it in the clinky category. Sample DH 2.4-2 was heated to 1200°C in air; slumping and surface melting were clearly observed. During this run, we began to worry about the effect of the oxygen atmosphere on the change in state of the slag from solid to liquid. The sample appeared to have developed an iron oxide 'skin' that might alter its melting properties. We changed to a nitrogen atmosphere to decrease the oxygen content within the furnace chamber from ~20% to ~2% by volume.

Sample DH 2.13 – 2 showed very little alteration after being heat treated. DH 2.14 - 2a appears not to have undergone much heat alteration. Some small portions of the sample expanded a little. DH 2.14 – 2b seems to have been affected in the same way as DH 2.14 – 2a. Sample DH 2.17 developed a fine bumpy reticulation (Fig. 45) similar to the reticulation pattern shown in the **Surface Morphologies** section. DH 2.19 became swollen to a great degree; a portion of the surface billowed into a large, rounded form. Its corners rounded as they melted. The surface of the sample became covered in small pores. In the DH 2.18 sample, the surface was partially affected by surface sweating.

The slags move through a progression of alterations as the temperature is raised. At approximately 1100°C the slags undergo surface sweating. They begin to slump in the range of temperatures between 1100 and 1150°C. The coarse slags appear to be less easily melted than the clinky and non-clinky slags. From these experiments, it appears that holding the slags for 15 minutes at 1100°C is insufficient to produce gross morphological changes, such as slumping. On the other hand, the non-clinky slag DH 2.19 was dramatically altered when held at 1150°C for a 10-minute soak. This result correlates well with the slag melting temperatures determined by the ternary phase diagram analyses (see Figs. 41, 42).

Most of the experimentally treated furnace slags developed a highly specular sheen. In addition, the samples seem to have lessened somewhat in density, most likely as a result of the development of air bubbles within the interior of the slags. Many of the samples

stuck to the alundum boat, indicating that at least some sweating/melting had taken place. Even at 1250°C these slags were clearly not completely molten, nor did they run freely.

The viscosity of these slags during the smelting process hindered the gravitational movement of the smelted copper and trapped prills during cooling and solidification. The melting temperature of the slags is likely to be somewhat higher than that calculated with the ternary phase diagram (Figs. 41 and 42). The slags are not composed of only these three pure components: SiO_2, Al_2O_3, FeO. They contain material that complicates and alters their thermal behavior. Even so, the furnace experiments corroborate the results obtained from the ternary phase diagram plot.

Discussion

For many years materials engineering laboratory studies of West Mexican metal artifacts have been carried out at MIT (Hosler 1988a,b, 1994, 1995). These provide concrete evidence of the metals and alloys used and of how the objects were designed and fabricated. What has been lacking, however, are studies of the stage of metallurgy that precedes object manufacture, that is, extractive metallurgical processes to win metal from its ores.

The discovery of the site of El Manchon represents the first opportunity for investigators to report on extractive metallurgy in Mesoamerica (Hosler 2003 a, b). Unfortunately, the smelting furnaces at the site are highly disturbed from tree root intrusion and are no longer intact. This means that the primary evidence at our disposal for reconstruction of the smelting processes at El Manchon are the slag and ore remains. The purpose of this thesis is to analyze the ore and slag remains with the ultimate goal of reconstruction of the extractive metallurgical processes carried out at El Manchon. In spite of the serious constraints on the data we had available for analysis, nevertheless we have been able to provide some critical elements in the smelting procedures that were used. Certain aspects of the extractive technology are now within the realm of explanation:

1. Composition of the furnace charge
2. Type and purity of the metal smelted in the furnace
3. Type and composition of the slags produced
4. Minimum operating temperature of the furnaces
5. Overall furnace efficiency

We found that the ores being smelted were copper oxides and carbonates such as cuprite and malachite. The furnaces were charged with a mixture of these ores and wood charcoal. The ore originated from an oxide deposit that had weathered from a complex copper sulfide – iron sulfide ore. The ore, which contained copper and iron oxides in association with rocky quartz, was primarily self-fluxing. The self-fluxing quality of the furnace charge leads us to the conclusion that the furnaces did not have to operate at a temperature in excess of about 1200°C to smelt effectively.

The resulting metal was unalloyed copper. The copper was fairly pure, but might have required a further refining step to eliminate the small amount of sulfide still remaining in the form of inclusions. This may have been achieved by remelting the metallic copper in a crucible in the presence of a small amount of slag so that the slag would act as a collector for impurities such as sulfides that remained in the metal. The environment would be oxidizing, but the slag would serve as a barrier between the copper and the open air, preventing copper oxide scale from forming on the metal while simultaneously removing the impurities.

The El Manchon furnace slags analyzed thus for are primarily crystalline and glassy fayalite ($2FeO{\cdot}SiO_2$). A small amount of the crystalline phase of tridymite has been observed in some of the slag interiors. The slag was viscous and trapped many metal prills within it. The metalworkers of El Manchon were smelting in the low temperature range of the SiO_2-FeO binary system. Whereas the viscosity of the slag was high enough

to trap metallic prills of copper, even at 1200°C, the fact that only about two percent of the copper was retained in the slag means that the operation was quite efficient for an ancient smelting process. It is clear that most of the copper was consolidated within the furnace. By comparison, at Batán Grande, a pre Hispanic north coast Peruvian smelting site, large accumulations of crushed and powdered slag were recovered during excavations. The smelting technology could not raise the furnace temperature high enough to render slag of a low enough viscosity to allow travel of the metal. The trapped prills were not consolidated, and had to be separated mechanically from the slag by crushing. The fact that no such accumulations of powdered slag have been identified at El Manchon and that all the smelting slags are solid wastes indicates that the extractive processes were achieving adequate separation between slag and metal; the efficiency of the operation was fairly high with good recovery of metal.

We found the minimum smelting temperature of the furnaces to be about 1150°C.We do not, however, know how the elevated temperatures were achieved. Blowpipes were commonly used for smelting in the north Andean region of South America. At the site of Batán Grande, the presence of refractory ceramic tips (called tuyeres) that attached to the ends of long tubes of cane confirms the use of blowpipes in the extractive metallurgical operations. No such evidence has been excavated yet at El Manchon. Excavators have noted a seasonal strong breeze that blows up the slope where the furnaces are located. They suggest that the furnaces could have operated through the mechanism of natural drafts. Until we can reconstruct or excavate an intact furnace, this problem will be hard to solve.

One of the primary issues still unsolved is the relationship between the "coarse" and "smooth" slags. The smooth slags are all uniform in thickness and are quite thin - about 0.5 cm in thickness. Originally we thought that these two slag morphologies might have represented different stages in the smelting process, i.e. that the thin smooth slags resulted from a subsequent refining stage and that the coarse variety was produced during the initial smelt. The similarity in their copper content and overall compositional similarity, however, lead us to believe that this is not the case. If not, then how were the two types related to one another within the furnace? This question may be easily answered by excavating an undisturbed furnace. Unfortunately, these are not yet in evidence at El Manchon.

We are also uncertain if the slags are furnace slags (cooled within the furnace) or tapped slags (waste material tapped out while still molten). The reticulated surface morphology that we have been able to recreate experimentally was formed in both slow-cooling and quick-cooling circumstances. Thus we feel that the reticulation could have been formed inside or outside the furnace, during cooling and solidification. The faint waviness evident on the surface of many of the smooth slags seem as if they could have been created by pouring the material out onto a flat surface and allowing it to cool. This seems unlikely, though, because the temperatures we have measured at which these slags slump, which correspond to the operating range of furnace smelting temperatures, do not produce runny slag, which is necessary for a tap furnace to function.

Crystalline and glassy fayalite phases were the primary slag phases formed; only a minute volume fraction of crystalline tridymite was found in any of the slags we examined. This means that the initial melt composition was within the fayalite phase field. As the melt cooled, crystalline fayalite formed, and the melt composition moved toward the border between the two phases, tridymite and fayalite. If the temperature necessary for tridymite formation had been achieved and sustained, a larger proportion of tridymite would have formed in the fayalite matrix. It seems, instead, that after the crystalline fayalite formed the rest of the melt solidified into the glassy phase we documented. This solidification behavior seems to provide a reasonable explanation for the formation of the clinky vs. non-clinky slags. Sound travels in the clinky slag in a manner akin to that of glass. It follows that the ratio of glassy to crystalline fayalite is probably higher in the pieces that sound more like glass: the smooth, clinky slags. Perhaps these slags were located in a zone of the furnace where they cooled more rapidly. The melt would not have had as much time to form crystalline fayalite before solidifying into glassy phases. The surface morphology that seems to have been produced by quick cooling --wrinkled/cracked-- is found primarily on the clinky slags. This further corroborates the possibility that the clinky slags were cooled more quickly than the non-clinky.

The wrinkled/cracked surface morphology exhibits a surface fraught with cracks and wrinkles produced by strain on cooling. It is our theory that this surface was cooled quickly in air, forming a solid 'skin' that floated on a semi-molten slag interior.

Perturbations in the lower molten region likely caused this pattern of disturbance on the surface.

The most common surface in all the smooth slags was one that exhibited a reticulated network. Two of the slag samples that were heated experimentally formed a reticulated surface where none had existed prior to heating. The reticulation that developed on the surface of the treated sample closely matches the reticulation found on other excavated slags. The creation of this surface leads us to believe that some of the surface morphologies characteristic of the Manchon slags are dependent on their thermal history. The reticulated morphology may represent surface sweating during heating and shrinkage upon subsequent cooling.

Elongated needle-like crystals characterize the acicular surface morphology. The pattern of this surface relates to fayalite crystal structures existent in the interior of the slag. The morphology of the interiors of these slags were observed with low-power microscopy and captured on photomicrographs. The similarity between the surface morphology and the microstructure indicates that the two are manifestations of the same features: fayalite crystals.

Our hope is that subsequent excavations at El Manchon can be guided by the results of this thesis to investigate further the technologies and organization of metal extraction, processing and production in Mesoamerica.

Further Work

The size of the furnaces at El Manchon is still unknown. If one were able to match some of the edge pieces of slag, like putting together a jigsaw puzzle, we might be able to determine the interior diameter of the furnaces and thus to calculate the likely volume of metal a furnace could have produced in a given firing. Measuring the viscosity of the slag would help assess how easily the metallic prills moved through the semi-molten material. A determination of the relative volume fractions of crystalline fayalite, glassy fayalite and crystalline tridymite would refine our evaluation of the circumstances under which the slags cooled. Comparing the relative amounts of glassy and crystalline material in the smooth slags would help determine if the percentage of glassy material vs. crystalline imparts different sound qualities to the different kinds of slag.

All the slags examined in this thesis were taken from only one of the levels (10-20 cm) of the slag heap excavated at El Manchon. Several deeper layers remain to be washed and examined. If the heap was deposited over a significant amount of time, the layers near the bottom might yield information to suggest that the process of smelting was refined and improved over time. Detailed analyses of slag at other levels could shed light on the progression of metallurgical technologies at El Manchon and in Mesoamerica. Further refinement of the data presented here as well as subsequent studies to investigate aspects of the smelting processes that may become evident upon further field research are essential in order to identify accurately what occurred in the extractive metallurgical industries of Mesoamerica.

Acknowledgements

I would like to take a moment to especially thank my thesis advisor, Professor Heather Lechtman, as well as my 3C advisor Professor Dorothy Hosler and the CMRAE laboratory supervisor Dr. Elizabeth Hendrix for all the help and support they gave in association with this project and in general.

In addition, many other people provided invaluable support to this project and I would like to mention them as well:

Professor Claude Lupis, DMSE

Professor Bernhard Wuensch, DMSE

Mr. Joseph Adario, DMSE

Dr. Harold Larson, DMSE

Mr. Donald Galler, DMSE

Professor Thomas Eagar, DMSE

Mr. Michael Tarkanian, DMSE

Dr. Nilanjan Chatterjee, EAPS

Dr. Henri Gaye, Dept. of Physical Chemistry, IRSID, France

Professor Yet-Ming Chiang, DMSE

Activation Laboratories, Canada

Mr. Sidney Carter, EAPS/Stanford University

THANK YOU!

References Cited

Allen, Gary, Judson, Sheldon, and Marvin Kauffman

1990 Physical Geology. 8th edition. pp. 420 – 433. Prentice Hall, Englewood Cliffs, New Jersey.

Bachmann, Hans-Gert

1980 Early copper smelting techniques in Sinai and in the Negev as deduced from slag investigations. *Scientific Studies in Early Mining and Extractive Metallurgy* (ed. P. Craddock). London: British Museum Occasional Paper No. 20. 103 -134.

1982 *The Identification of Slags from Archaeological Sites.* The Institute of Archaeology Occasional Publication No. 6, London.

Bateman, Alan M.

1951 The Formation of Mineral Deposits. pp. 227 - 245. John Wiley and Sons. New York.

Bowen, N. L. and J. F. Schairer

1932 SiO_2-FeO Phase Diagram. *American Journal of Science*, 5(24), 177-213.

Callister, William D. Jr.

2000 Materials Science and Engineering: An Introduction, 5th edition. Wiley and Sons: New York.

Chatterjee, Nilanjan

2001 Application of the Electron Microprobe in Mineralogy. *Microscopy Today*, vol. 1(6), July/August.

Chernicoff, Stanley and Donna Whitney

2002 Geology: An Introduction to Physical Geology. 3rd edition. pp. 634 – 640. Houghton Mifflin Company, Boston.

Ciliberto and Spoto, eds.

2000 Modern Analytical Methods in Art and Archaeology. Wiley-Interscience: New York.

Dietrich, Richard V. and Brian J. Skinner

1979 Rocks and Rock Minerals. pp. 274 - 285. John Wiley and Sons. New York.

Gill, Robin, ed.

1997 Modern Analytical Geochemistry: An Introduction to Quantitative Chemical Analysis Techniques for Earth, Environmental and Material Scientists. Addison Wesley Longman Limited: London, England.

Graffam, G., Rivera, M., and Carevic, A.

1994 Copper Smelting in the Atacama: Ancient Metallurgy at the Ramaditas Site, Northern Chile. In In Quest of Mineral Wealth: Aboriginal and Colonial Mining and Metallurgy in Spanish America, eds. A.K. Craig and R.C. West, Geoscience and Man, vol. 33, pp. 75-92.

1996 Ancient Metallurgy in the Atacama: Evidence for Copper Smelting during Chile's Early Ceramic Period. Latin American Antiquity 7 (2): 101-113.

Hauptmann, Andreas

1989 The Earliest Periods of Copper Metallurgy in Feinan, Jordan. pp. 119-135. Old World Archaeometallurgy. Andreas Hauptmann, Ernst Pernicka, and Günther A. Wagner, eds. Bergbau-Museum, Bochum.

Hosler, Dorothy

1988a Ancient West Mexican Metallurgy: A Technological Chronology. *Journal of Field Archaeology* 15:191-217.

1988b Ancient West Mexican Metallurgy: South and Central American Origins and West Mexican Transformations. *American Anthropologist* 90(4):832-855.

1994 The Sounds and Colors of Power: The Sacred Metallurgical Technology of Ancient West Mexico. The MIT Press. Cambridge, Massachusetts.

1995 Sound, color and meaning in the metallurgy of Ancient West Mexico. *World Archeology* 27(1):100-15.

2003a "Topographical and Archaeological Maps of Two Ancient Mexican Copper Smelting and Production sites." (excerpts from a grant proposal; Dorothy Hosler, personal communications, April 2003).

2003b "Nuestros Hallazgos en la Metalurgia de Guerrero." La Arqueología del Estado de Guerrero. El Gobierno del Estado de Guerrero.

Hosler, Dorothy, Lechtman, Heather, and Holm, Olaf

1990 *Axe-monies and their Relatives,*. Dumbarton Oaks Research Library and Collection, Washington, D.C.

Jenkins, Neil

2001 Excavation Notes from El Manchon, 15.i.01 through 24.i.01.

Lechtman, Heather N.

1979 "A Pre-Columbian Technique for Electrochemical Replacement Plating of Gold and Silver on Copper Objects," *Journal of Metals* 31:154-60.
1984 "Pre-Columbian Surface Metallurgy," *Scientific American* 250:56-63.
1988 "Traditions and Styles in Central Andean Metalworking." In The Beginning of the Use of Metals and Alloys, Robert Maddin, ed. Cambridge: MIT Press, pp. 344-378.
1991 "The Production of Copper-Arsenic Alloys in the Central Andes: Highland Ores and Coastal Smelters?," *Journal of Field Archaeology* 18(1):43-76.
1993 "Technologies of Power - The Andean Case." In Configurations of Power In Complex Society, John S. Henderson and Patricia J. Netherly, eds. Ithaca: Cornell University Press, pp. 244-280.
1996 "Arsenic Bronze: Dirty Copper of Chosen Alloy?." *Journal of Field Archaeology* 23: 477-514.
2002 "Tiwanaku Period (Middle Horizon) Bronze Metallurgy in the Lake Titicaca Basin: A Preliminary Assessment." In Tiwanaku and Its Hinterland, Vol. 2, Alan Kolata, ed. Washington, D.C.: Smithsonian Institution Press, pp. 404-434.

Lechtman, Heather N. and Sabine Klein

1999 Production of Copper-Arsenic Alloys (Arsenic Bronze) by Cosmelting: Modern Experiment, Ancient Practice. *Journal of Archaeological Science* 26: 497-526.

Lehmann, J., H. Gaye, W. Yamada, and T. Matusmiya

1990 A Statistical thermodynamics model of sulphur and fluorine bearing iron- and steelmaking slags. Proceedings of The Sixth International Iron and Steel Congress, Nagoya, ISIJ.

Merkel, John and Izumi Shimada

1988 Arsenical Copper Smelting at Batan Grande, Peru. Institute for Archaeo-Metallurgical Studies Newsletter 2: 4-7.

Rapp, Jr., George

1998 Composition and Softening/fluid Temperatures of Some Ancient Cypriot slags. pp. 177 – 182. Metallurgica Antiqua. Thilo Rehren, Andreas Hauptmann, James D. Muhly, eds. Bergbau-Museum, Bochum.

Rehder, J.E.

1994 Blowpipes versus Bellows in Ancient Metallurgy. *Journal of Field Archaeology* 21:345-350.

Rittau, Adrienne I.

2002 Personal Communication. ICP Technical Manager at Activation Labs, Ontario, Canada.

Rudolph, Stephan

2000 http://www.a-m.de/englisch/lexikon/mineral/oxide/tridymit.htm Büro für angewandte Mineralogie, Tönisvorst, Deutschland.

Segal, Irina, Beno Rothenberg and Miriam Bar-Matthews

1998 Smelting Slags from Prehistoric Sites F2 and N3 in Timna, SW Arabah, Israel. pp. 223-234. Metallurgica Antiqua. Thilo Rehren, Andreas Hauptmann, James D. Muhly, eds. Bergbau-Museum, Bochum.

Shimada, Izumi

1985 Perception, Procurement, and Management of Resources: Archaeological Perspective. In Andean Ecology and Civilization. Shozo Masuda, Izumi Shimada, and Craig Morris, eds. pp. 357-399. Tokyo: University of Tokyo Press.

Shimada, I., Epstein, S.M., and Craig, A.K.

1982 Batán Grande: A prehistoric metallurgical center in Peru. *Science* 216: 952 - 959.

1983 The metallurgical process in ancient north Peru. *Archaeology* 36(5): 38-45.

Stos-Gale, Sophie, George Maliotis and Noel Gale

1998 A Preliminary Survey of the Cypriot Slag Heaps and Their Contribution to the Reconstruction of Copper Production on Cyprus. pp. 235-262. Metallurgica Antiqua. Thilo Rehren, Andreas Hauptmann, James D. Muhly, eds. Bergbau-Museum, Bochum.

Stos-Gale, Zofia Anna

1989 Cycladic Copper Metallurgy. pp. 279-291. Old World Archaeometallurgy. Andreas Hauptmann, Ernst Pernicka, and Günther A. Wagner, eds. Bergbau-Museum, Bochum.

Todd, I. A.

1976 Catal Huyuk in Perspective. Cummings Publishing Company, Menlo Park, California.

Townsend, Richard F., ed.

1998 Ancient West Mexico: Art and Archaeology of the Unknown Past. The Art Institute of Chicago, Chicago, IL.

West, Robert C.

1994 "Aboriginal Metallurgy and Metalworking in Spanish America: A Brief Overview," In *In Quest of Mineral Wealth: Aboriginal and Colonial Mining and Metallurgy in Spanish America.* Alan K. Craig and Robert C West, eds. pp. 5-20. *Geoscience and Man*, volume 33. Geoscience Publications, Baton Rouge, Louisiana.

Zwicker, U., H. Greiner, K-H Hofmann, and M. Reithinger

1985 Smelting, Refining and Alloying of Copper and Copper Alloys in Crucible Furnaces During Prehistoric Up to Roman Times. In Furnaces and Smelting Technology in Antiquity. P.T. Craddock and M.J. Hughes, editors. British Museum, London. pp. 103-121.

Figure 1. Map of West Mexico and Coyuca Survey (Hosler, personal communication 2003).

Figure 2. Map of location of El Manchon and topographic map of Mesoamcerica, showing the limits of the West Mexican Metalworking Zone (Hosler 1994).

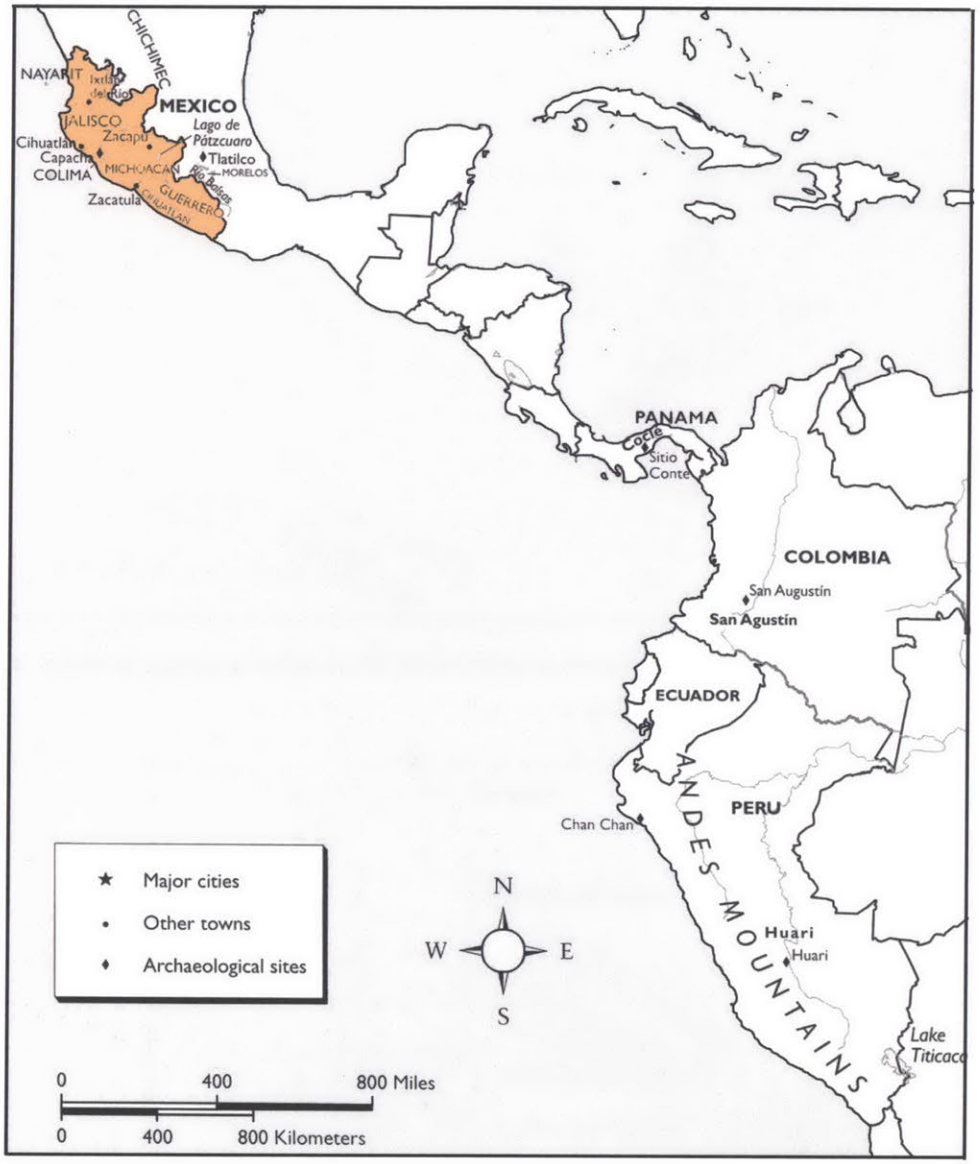

Figure 3. Map of the Pacific Coast from West Mexico to Peru (Townsend 1998, Fig. 2).

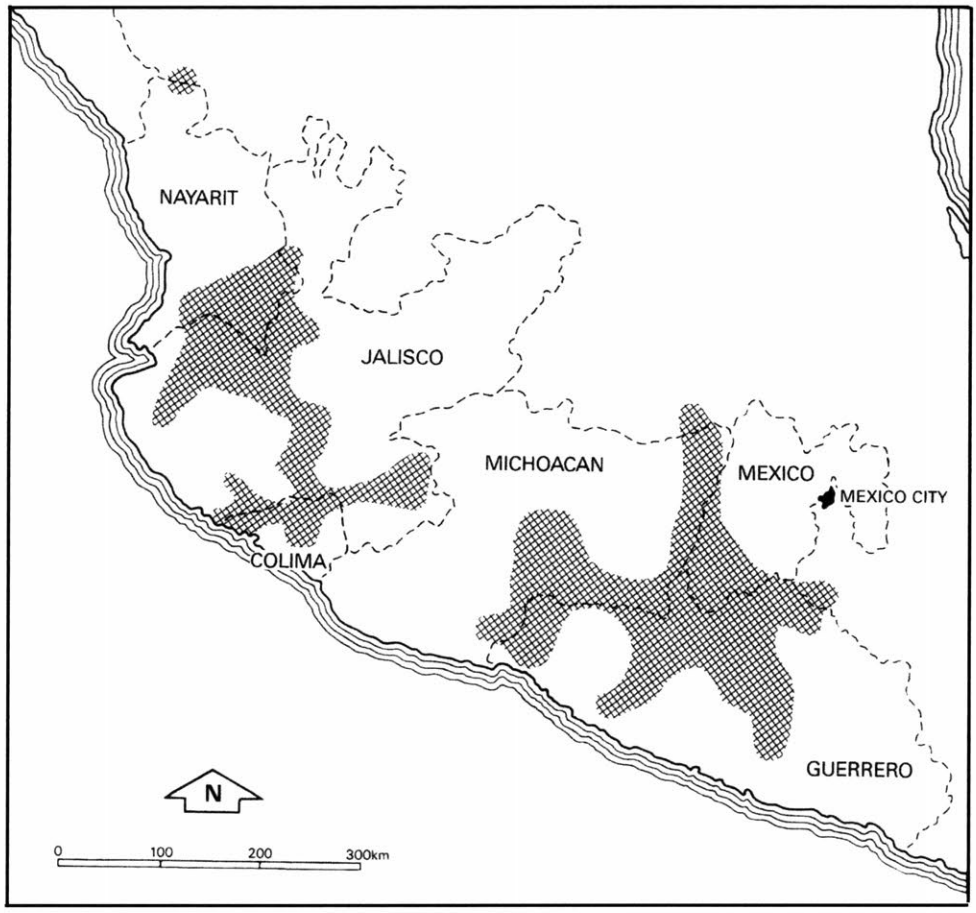

Figure 4. Zones of copper deposits in the West Mexican Metalworking Zone (Hosler 1994, Fig. 2.1).

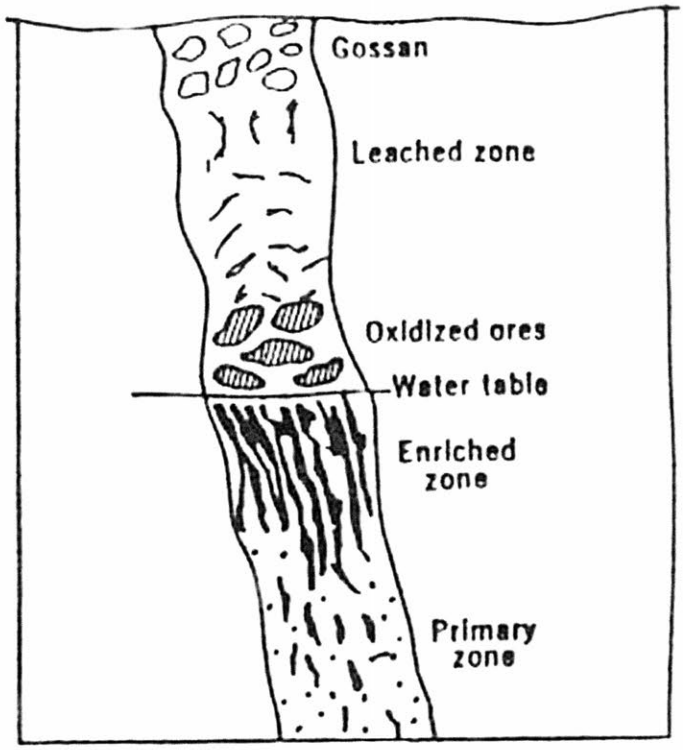

Figure 5. Diagram of zones of a weathered copper vein, showing the relation of oxidation and enrichment zones to the water table (from Bateman 1951, Fig. 11-6).

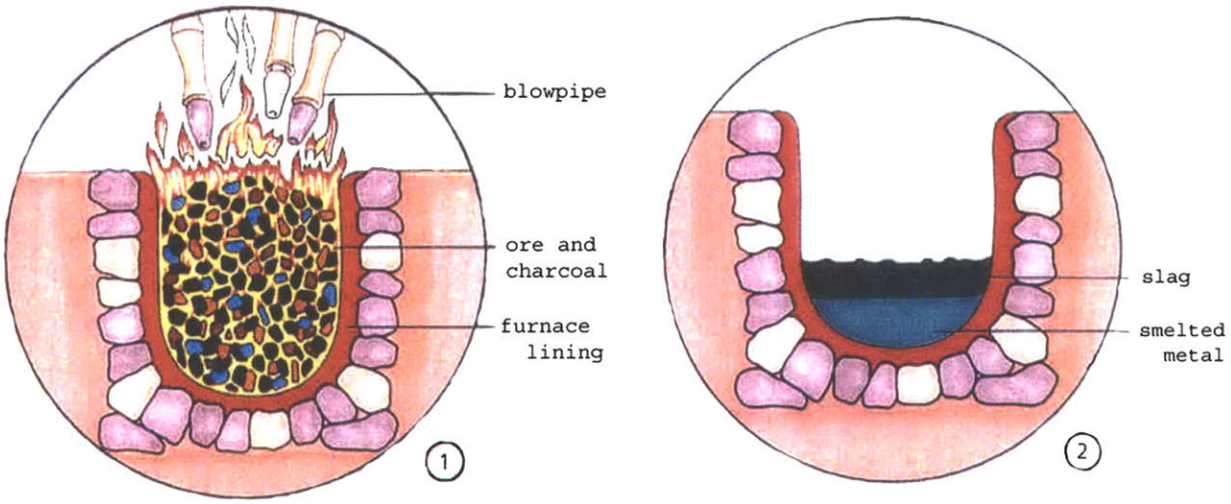

Figure 6. Simple bowl furnace of the type used in the Central Andes, before and after smelting operation (courtesy of Prof. Heather Lechtman).

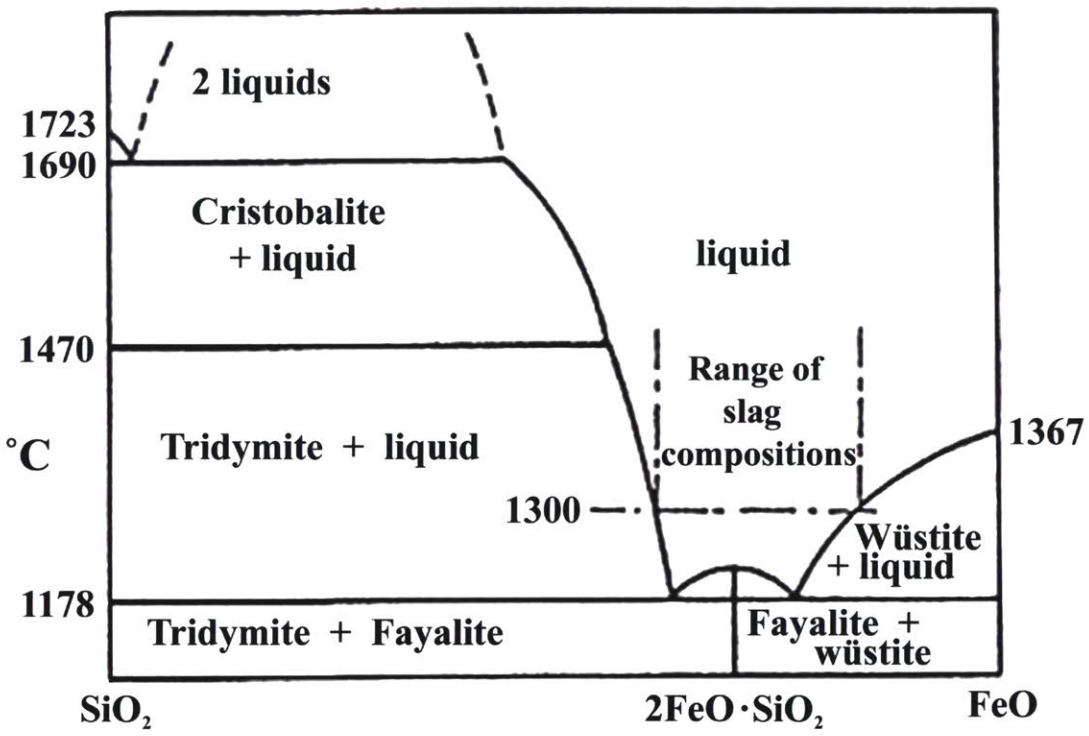

Figure 7. Equilibrium diagram of the system FeO-SiO2 (Bowen and Schairer 1932).

Figure 8. Assemblage of some ores excavated at El Manchon.

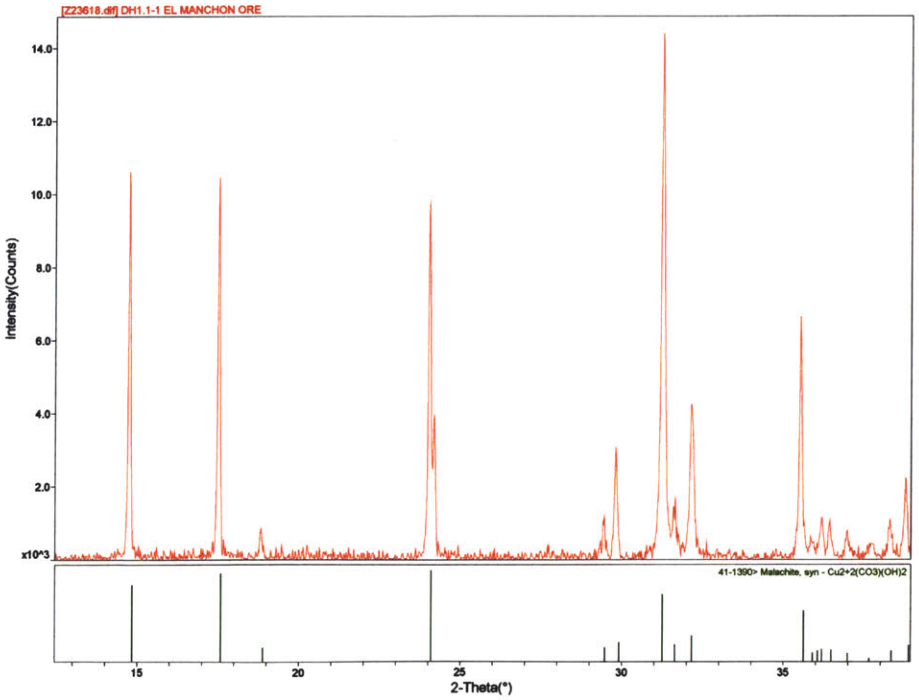

Figure 9. DH 1.1: XRD spectrum with malachite standard.

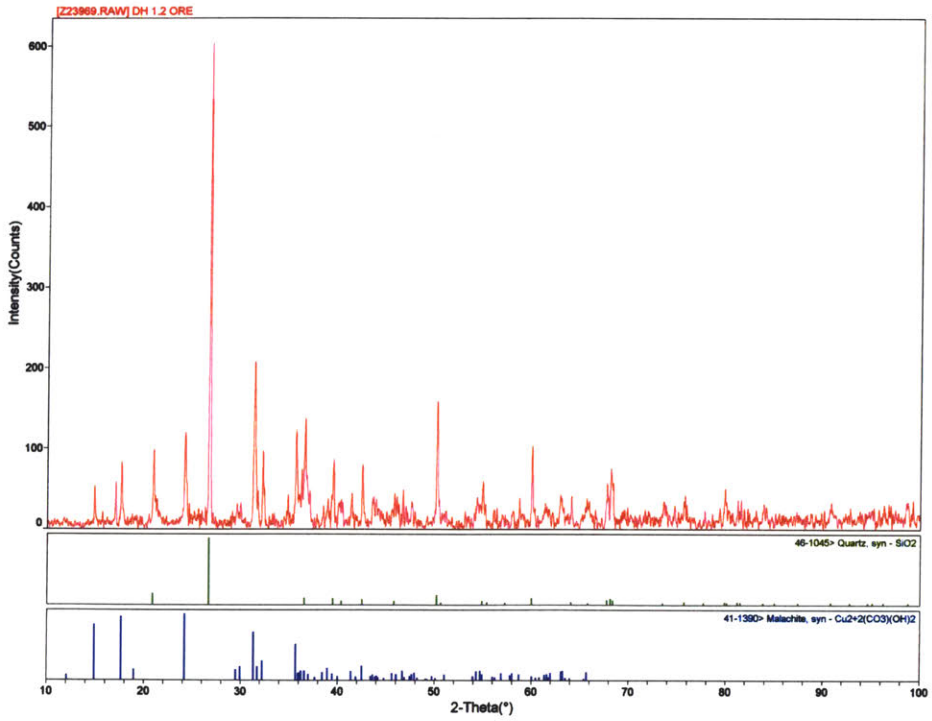

Figure 10. DH 1.2: XRD spectrum with malachite and quartz standards.

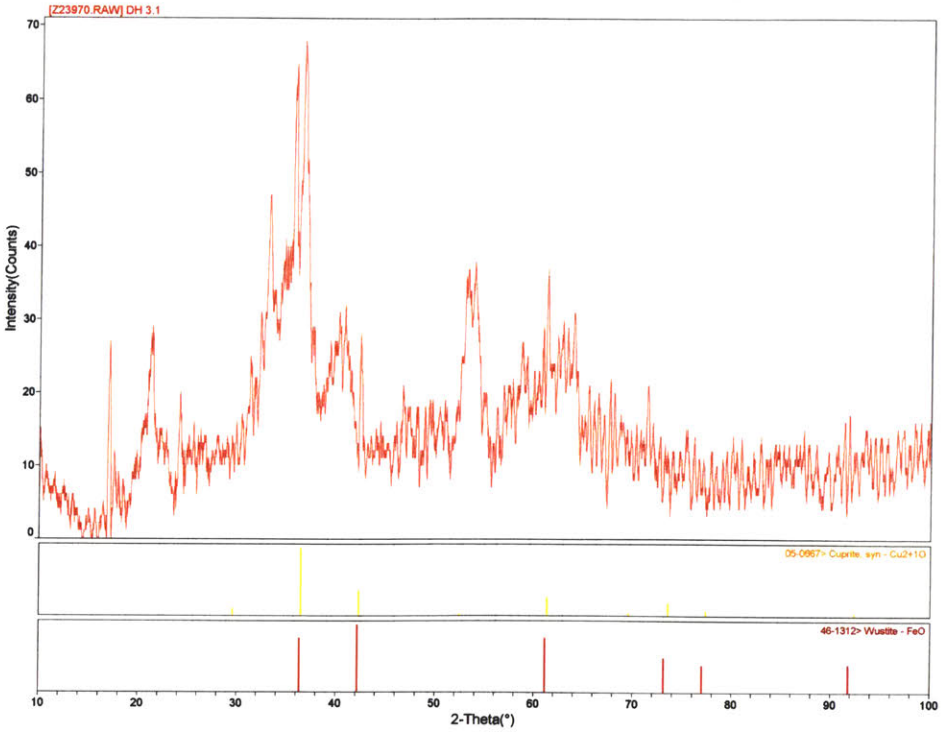

Figure 11. DH 3.1: XRD spectrum with cuprite and wüstite standards.

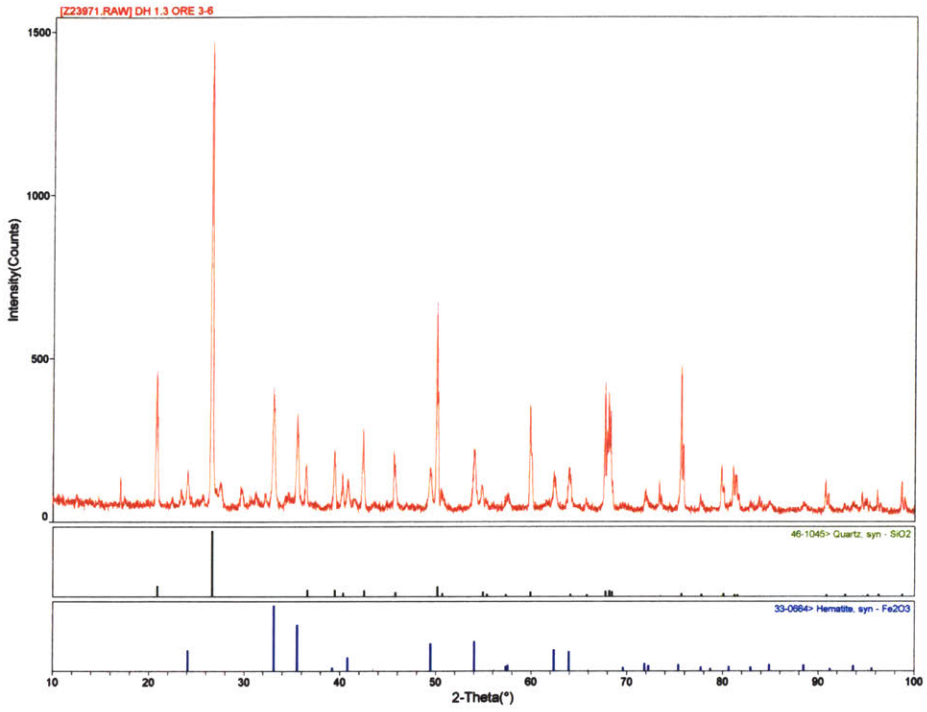

Figure 12. DH 1.3: XRD spectrum with quartz and hematite standards.

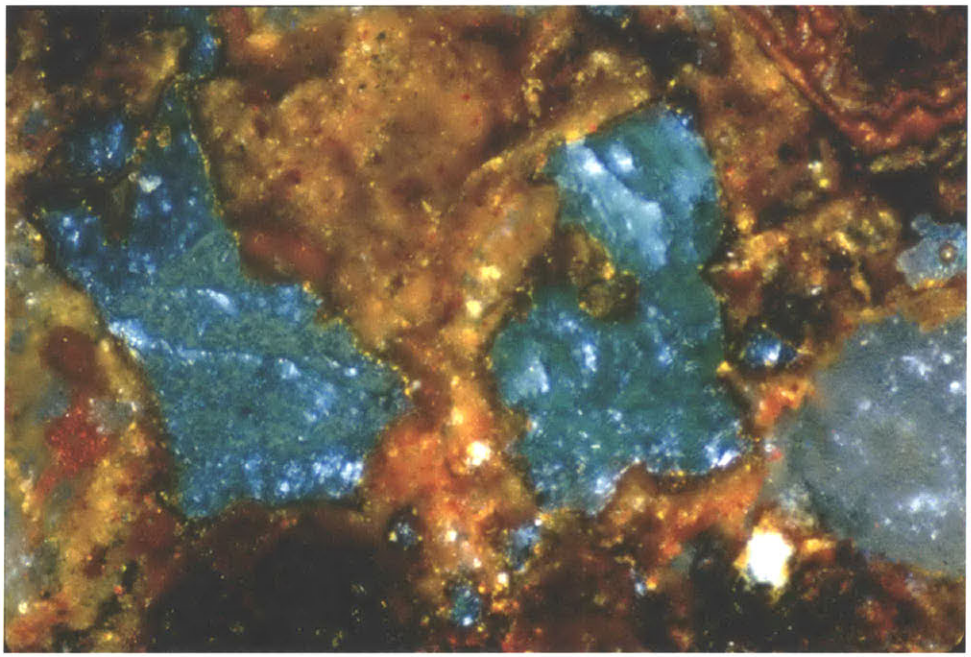

Figure 13. Ore 4-13: Thin section micrograph of red- and green-colored minerals under cross polarization (50x).

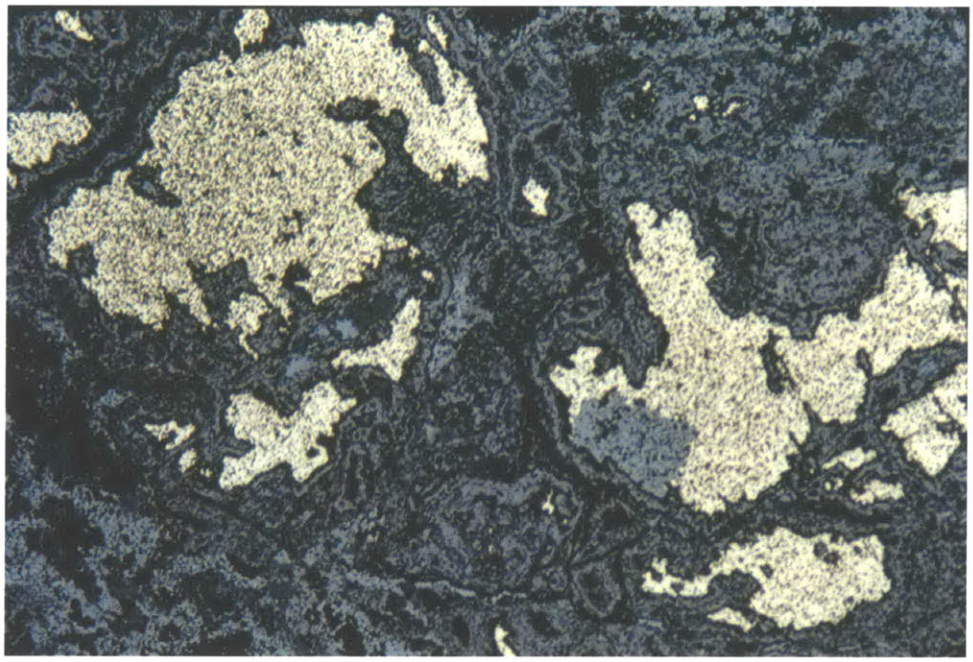

Figure 14. Ore 4-13: Thin section micrograph of golden opaque material with gray inclusion (50x).

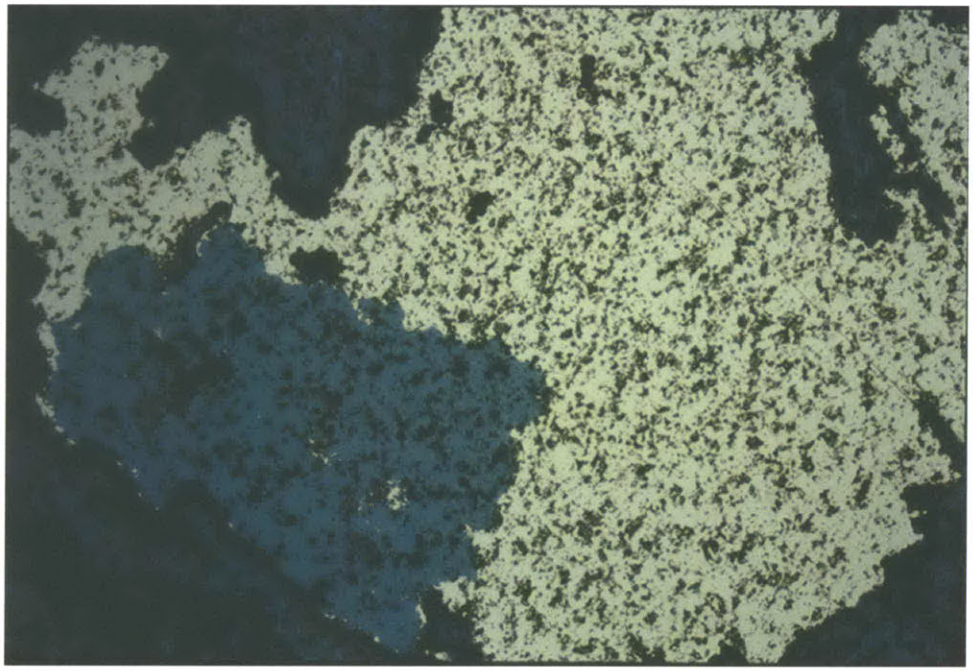

Figure 15. Ore 4-13: Thin section micrograph of golden opaque material with gray inclusion (200x).

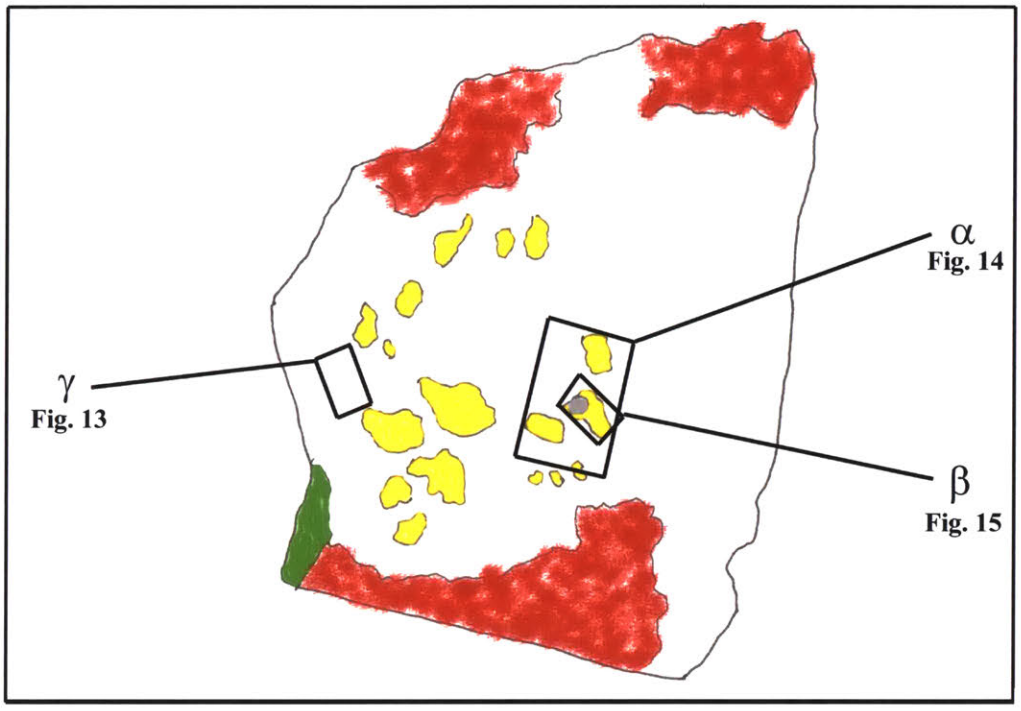

Figure 16. Ore 4-13: Map of locations within the thin section of micrographs shown in Figures 13, 14, and 15.

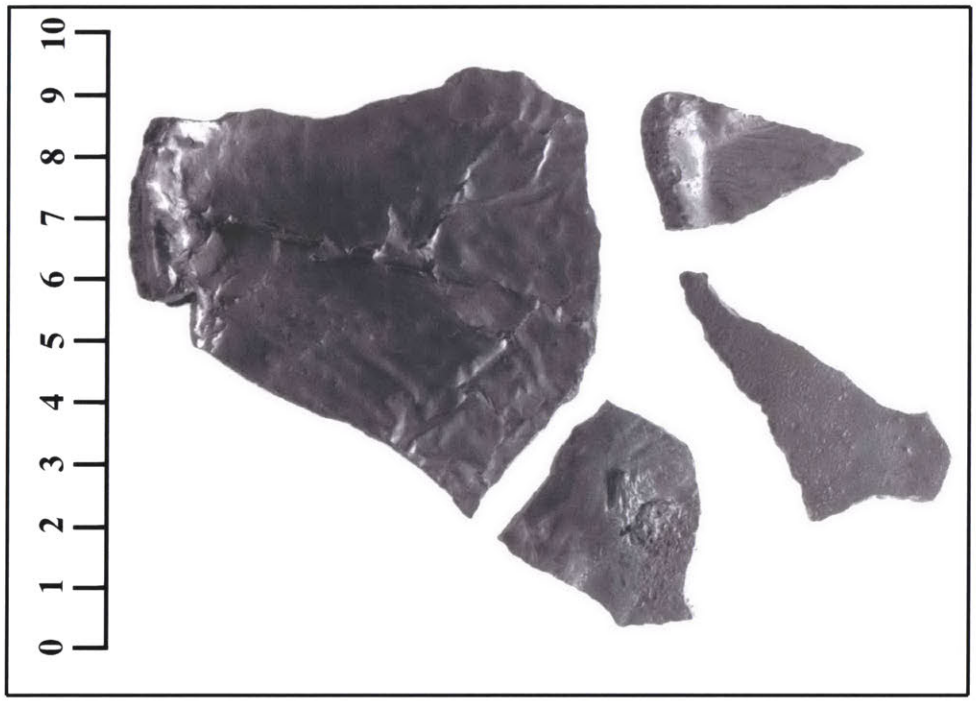

Figure 17. Smooth, clinky slags, El Manchon.

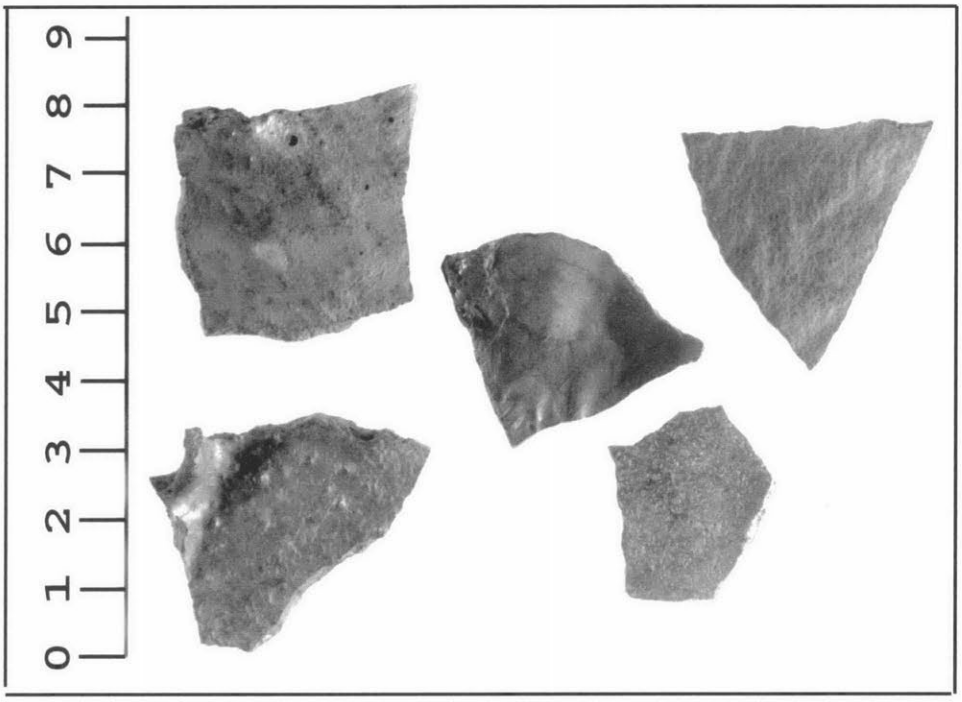

Figure 18. Smooth, non-clinky slags, El Manchon.

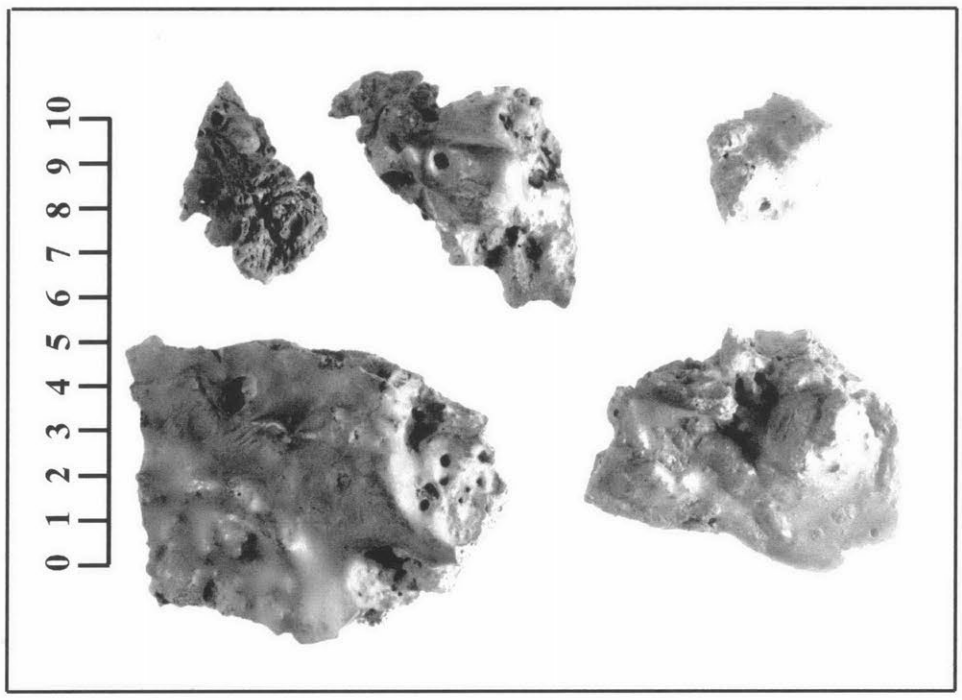

Figure 19. Coarse slags, El Manchon.

Figure 20. DH 2.2: Wrinkled cracked surface (x10).

Figure 21. DH 2.1: Reticulated surface (x10).

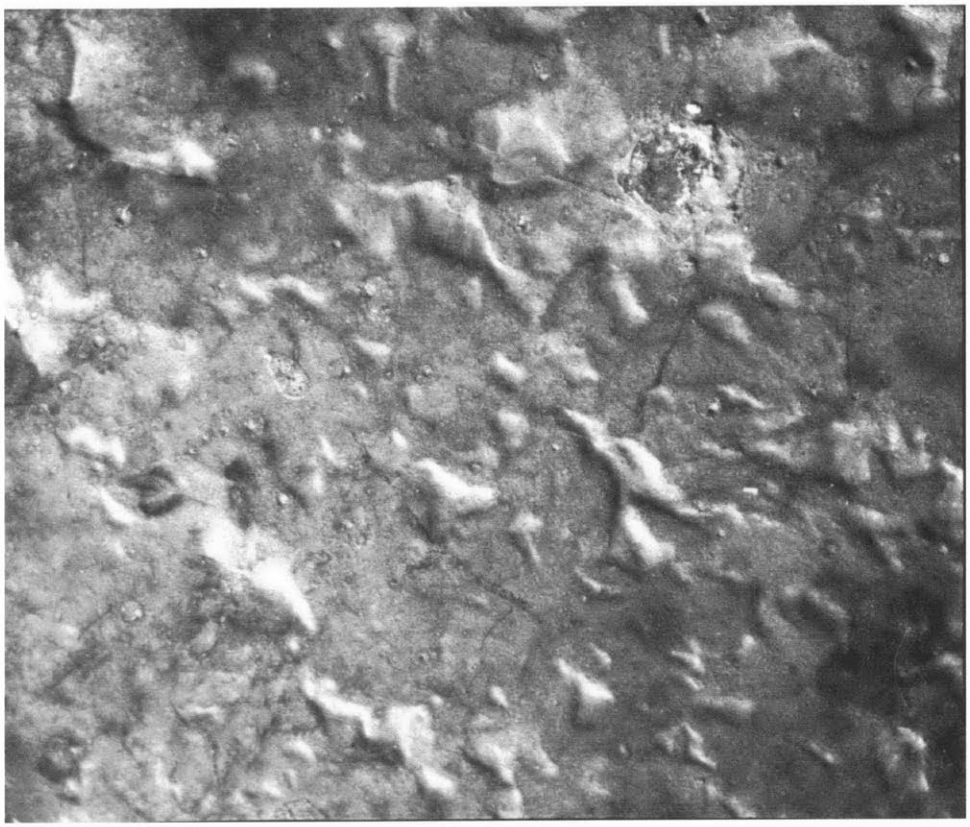

Figure 22. DH 2.5: Spongy surface (x10).

Figure 23. DH 2.8: Corroded surface (x10).

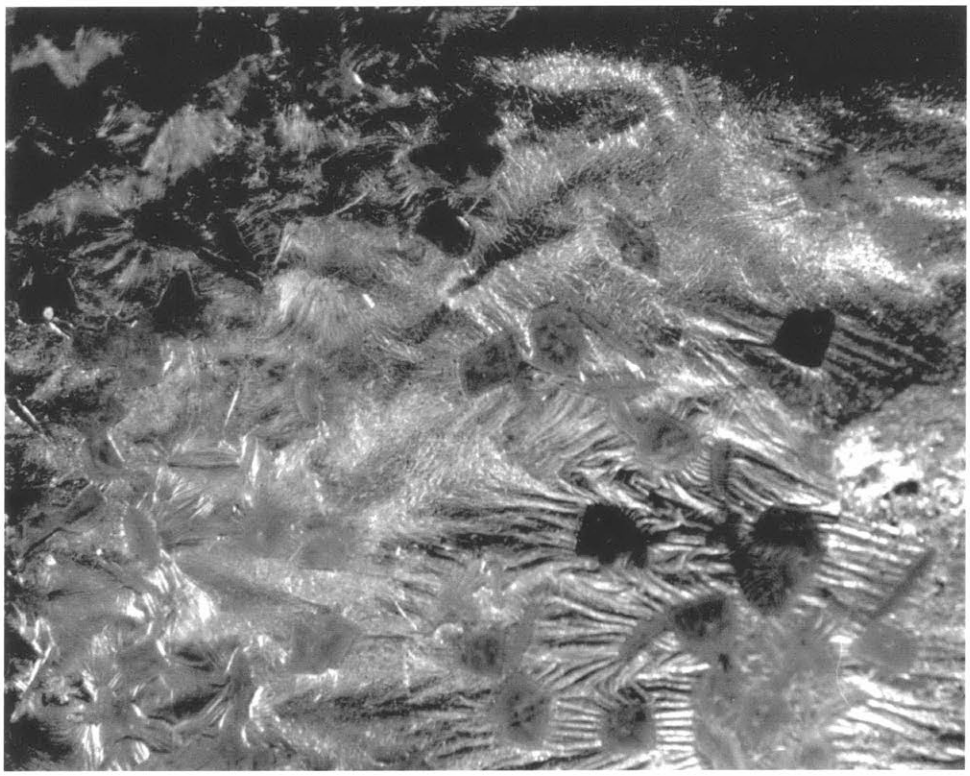

Figure 24. DH 2.1: Advanced grain growth surface (x10).

Figure 25. DH 2.3: Pink ridged, streaked surface (x10).

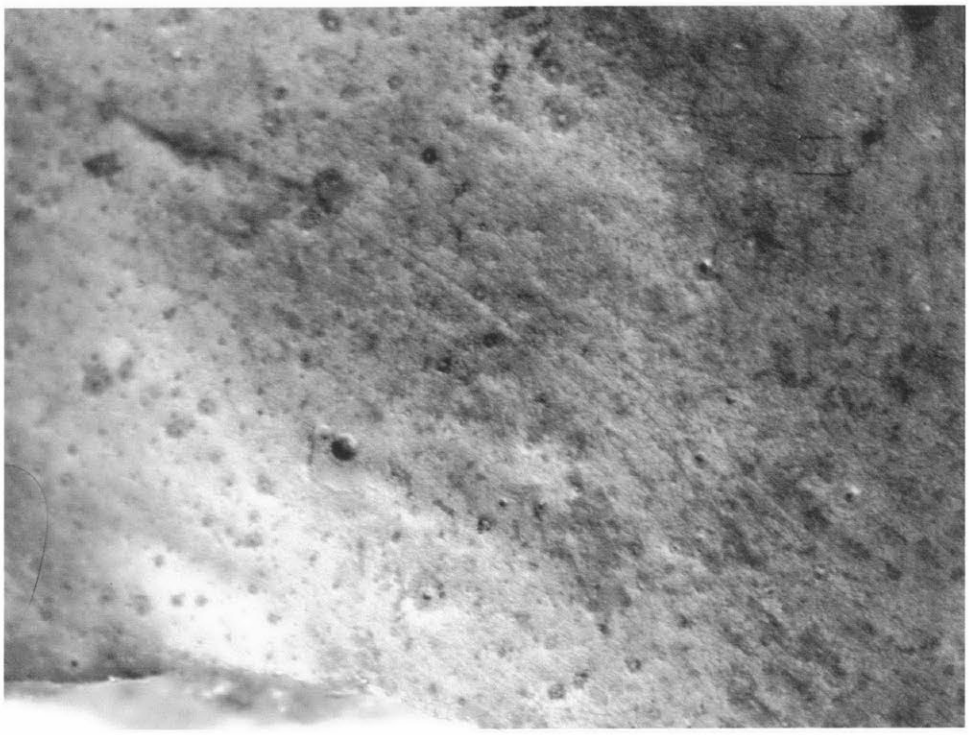

Figure 26.DH 2.7: Ridged, ringed pores and bumpy surface (x10).

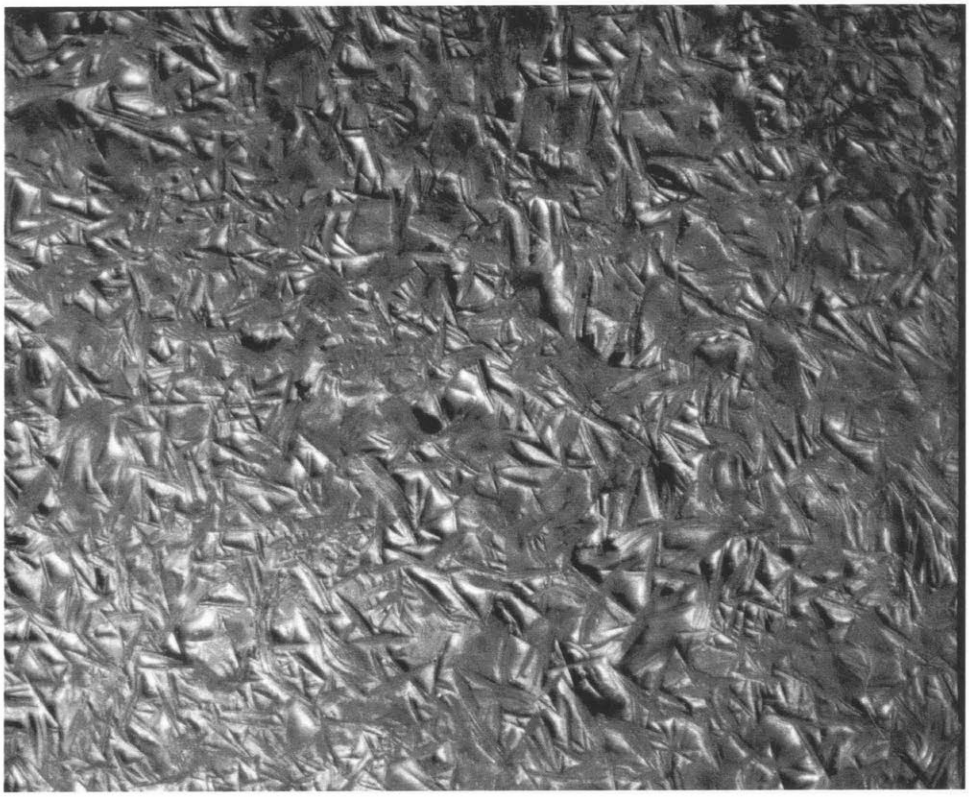

Figure 27. DH 2.4: Acicular surface (x10).

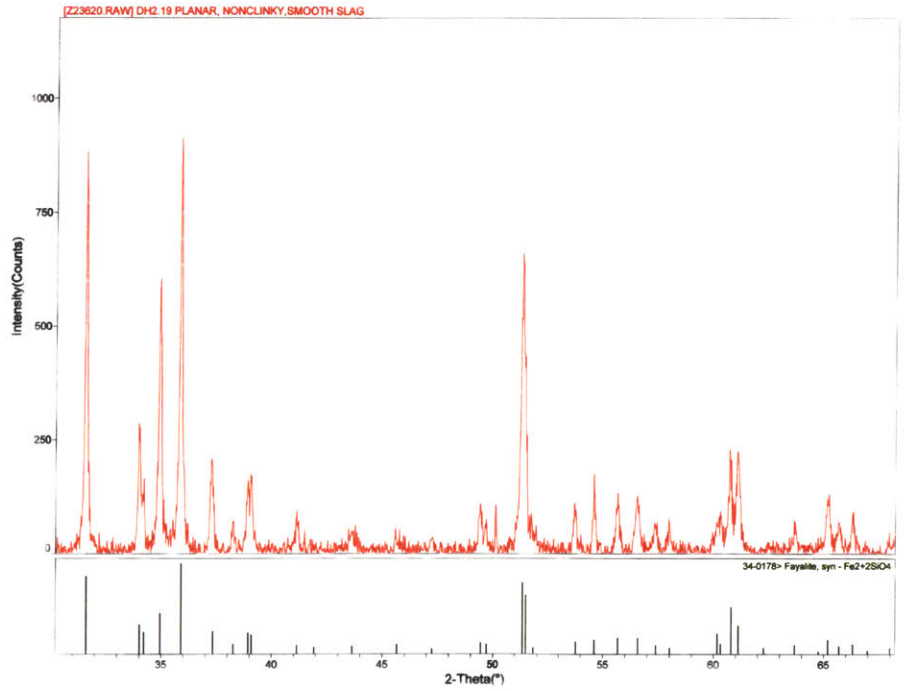

Figure 28. DH 2.19: XRD spectrum with fayalite standard.

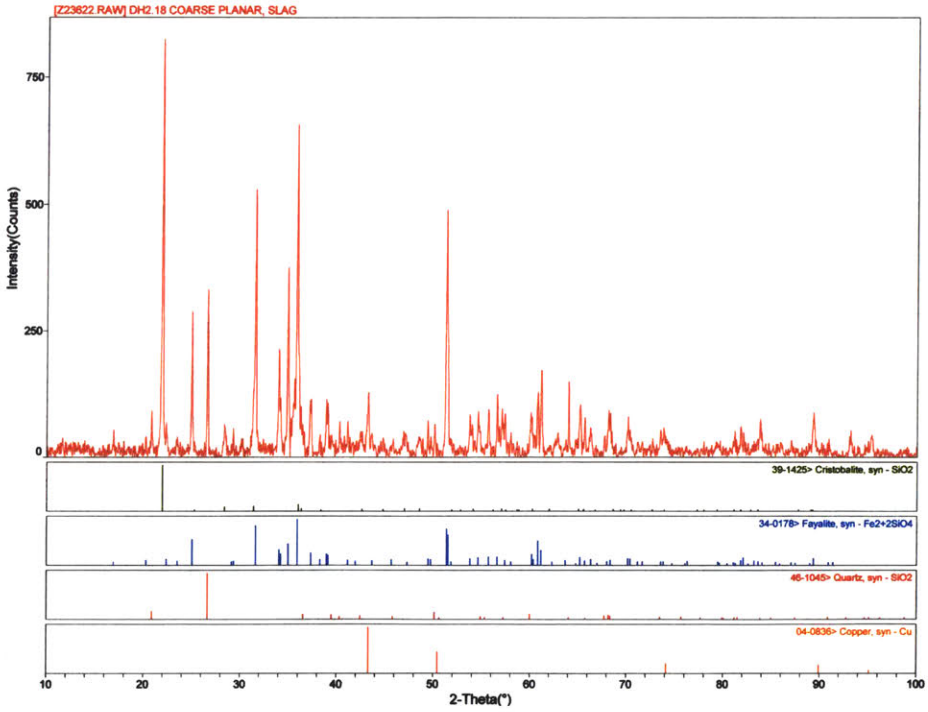

Figure 29. DH 2.18: XRD spectrum with cristobalite, fayalite, quartz and copper standards.

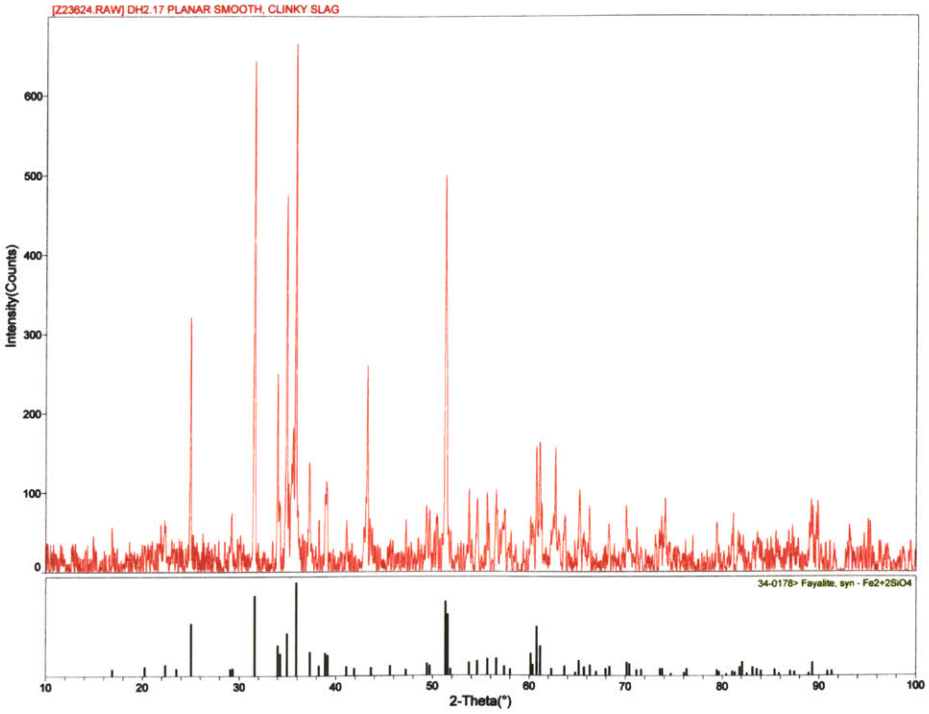

Figure 30. DH 2.17: XRD spectrum with fayalite standard.

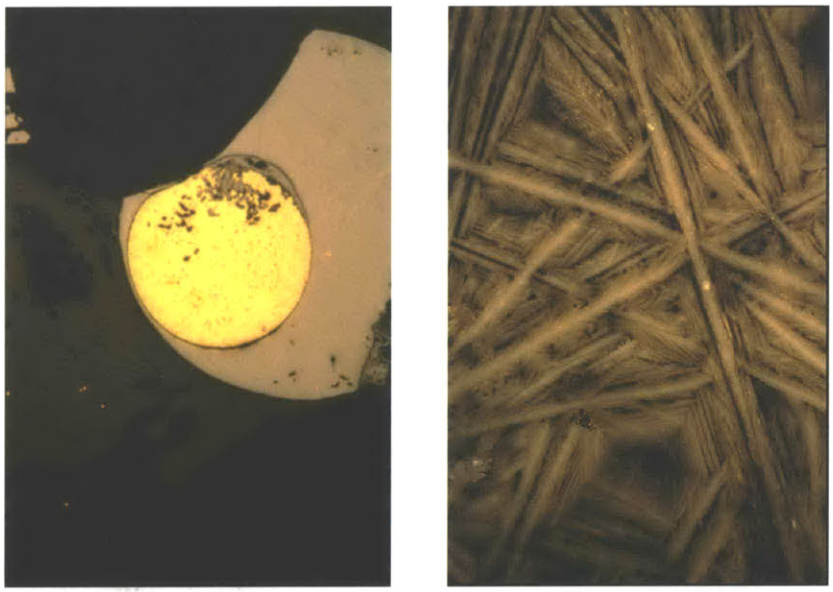

Figure 31. MIT 5258-A: Opaque section micrographs of copper prill and matte (left) and crystalline fayalite (right).

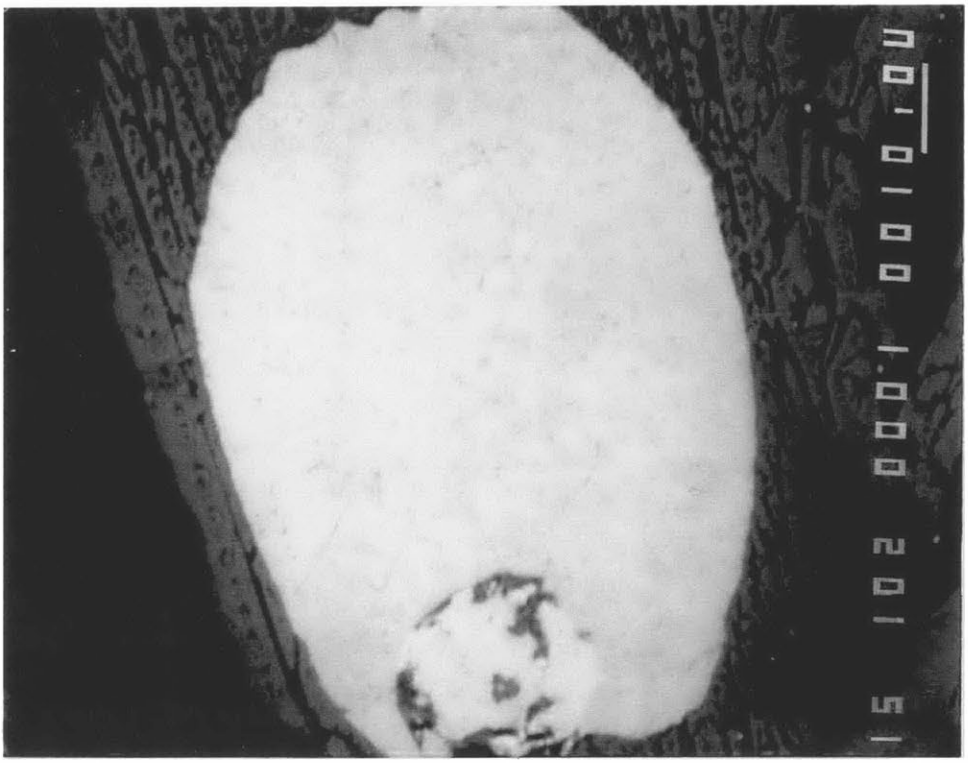

Figure 32. DH 2.1-1: SEM image of copper prill and matte.

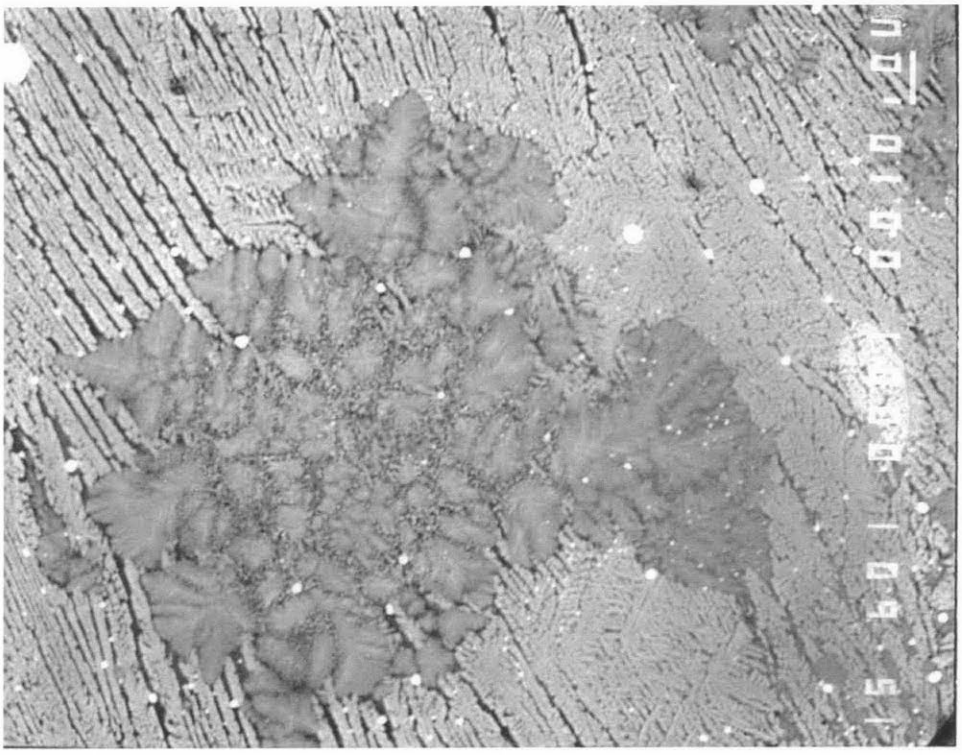

Figure 33. DH 2.13-1: SEM image of crystalline and glassy slag.

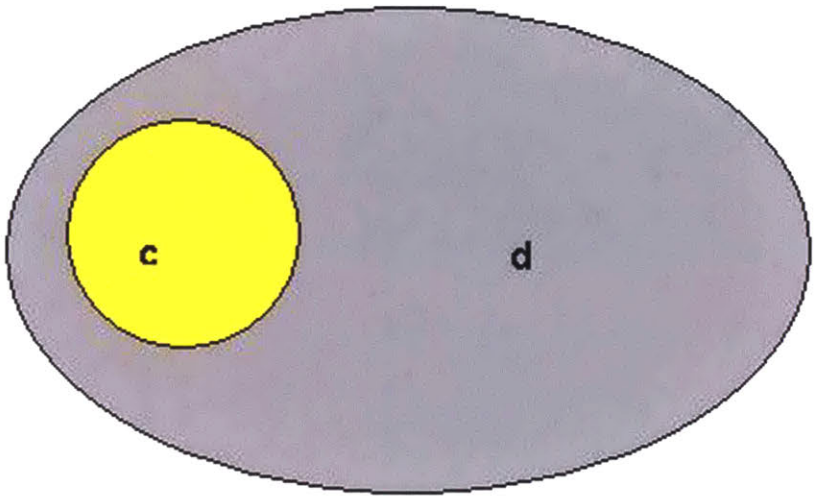

Figure 34. DH 2.13-1: Schematic indicating relative size and location of copper prill and matte.

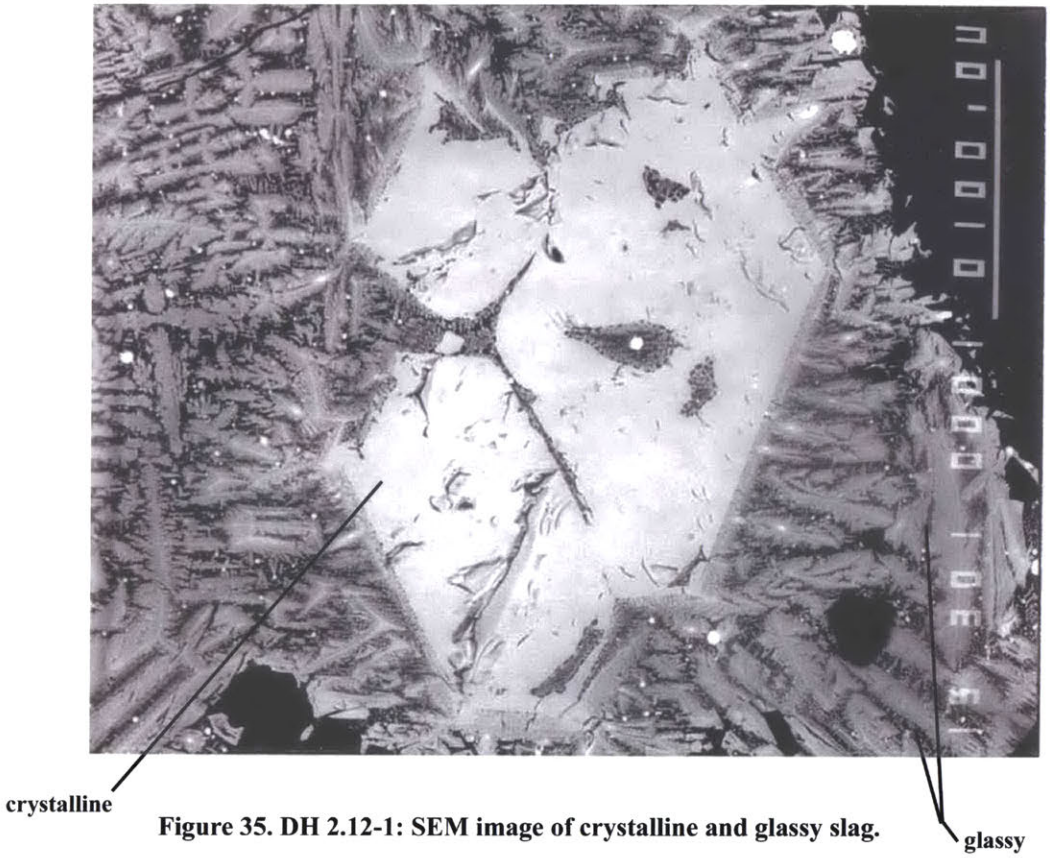

Figure 35. DH 2.12-1: SEM image of crystalline and glassy slag.

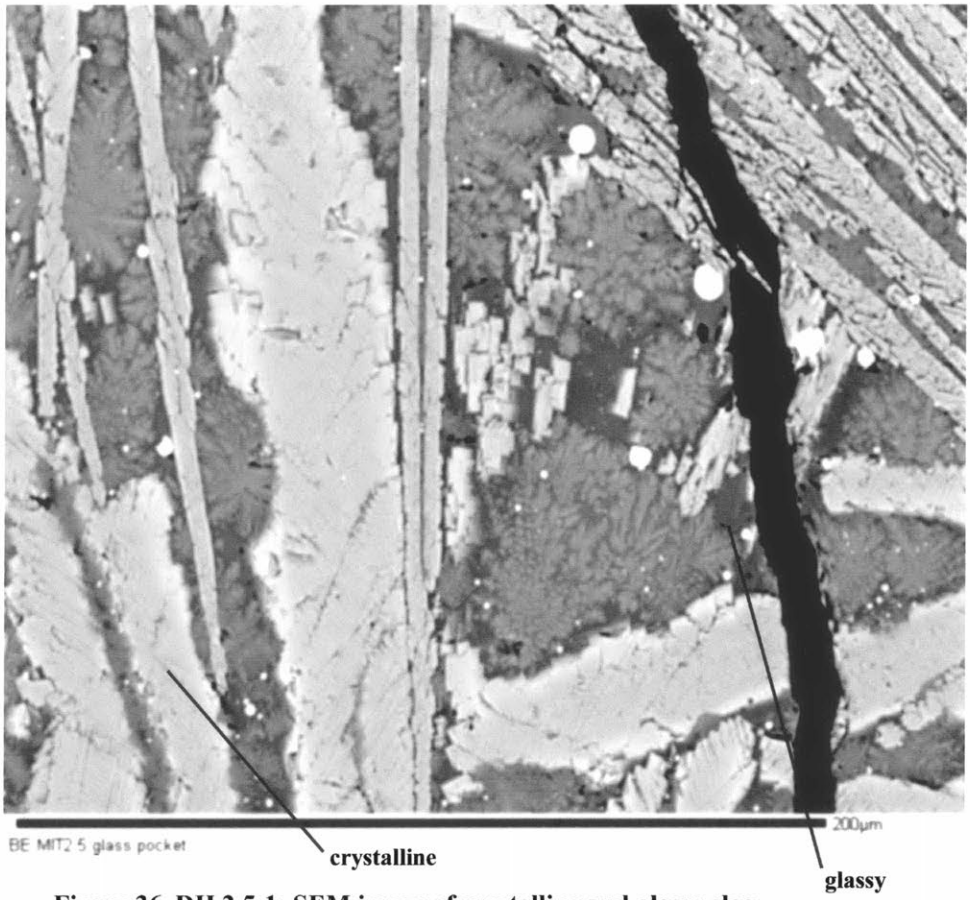

Figure 36. DH 2.5-1: SEM image of crystalline and glassy slag.

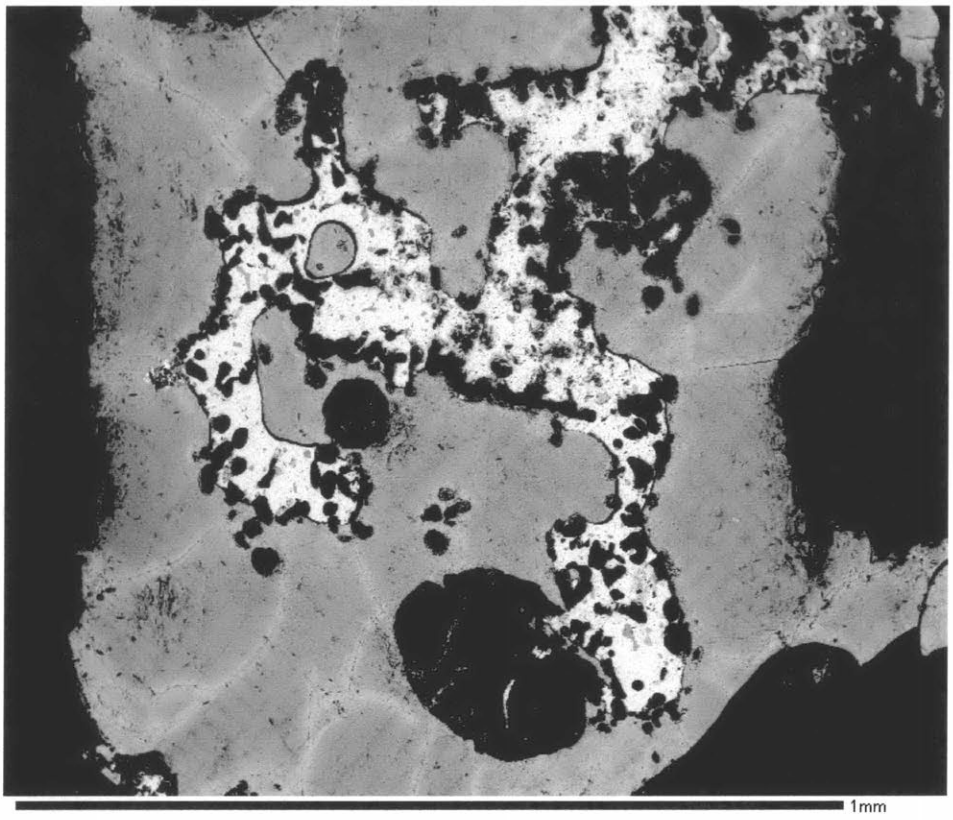

Figure 37. DH 2.14 – 1: SEM image of dark and light glassy slag.

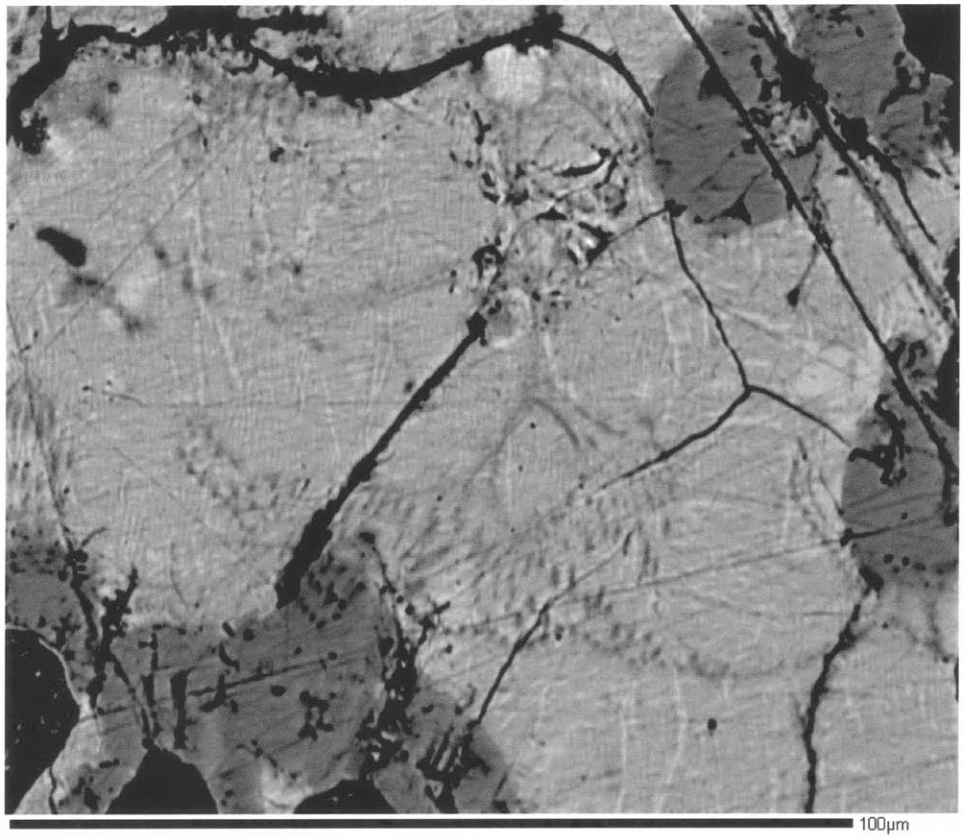

Figure 38. DH 2.14 – 1: SEM image of dark and light glassy slag; higher magnification detail of Figure 37.

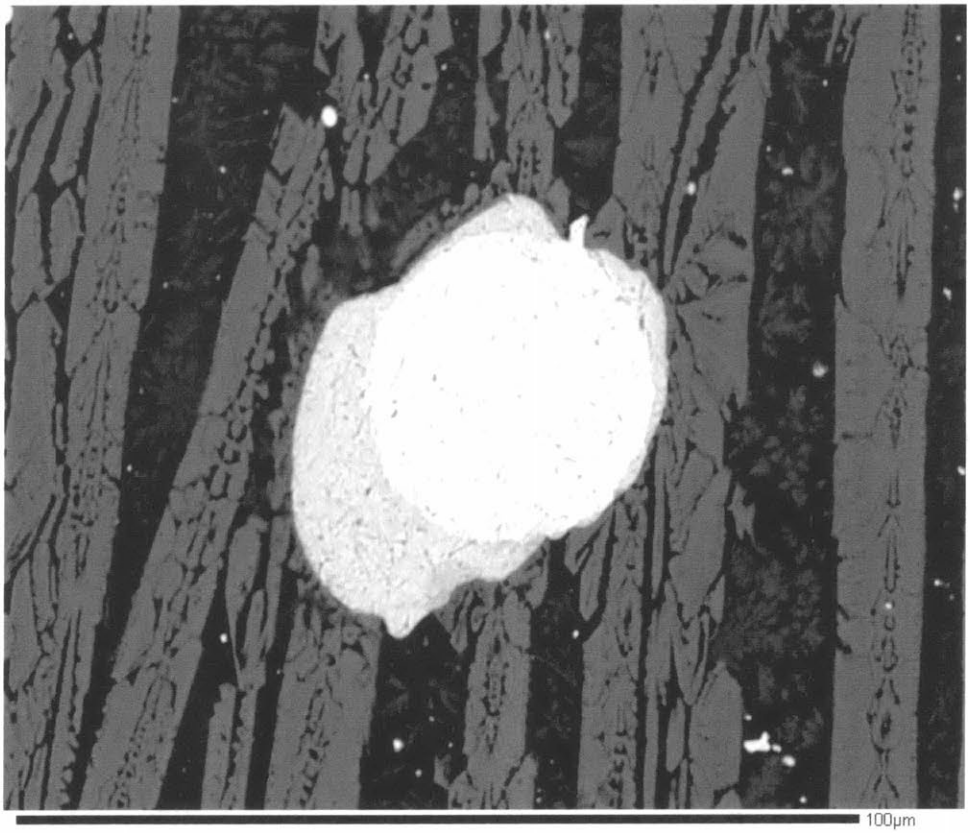

Figure 39. DH 2.15-1: SEM image of copper prill and matte.

Figure 40. DH 2.15 - 1: SEM image of crystalline and glassy slag, showing typical square tridymite crystals.

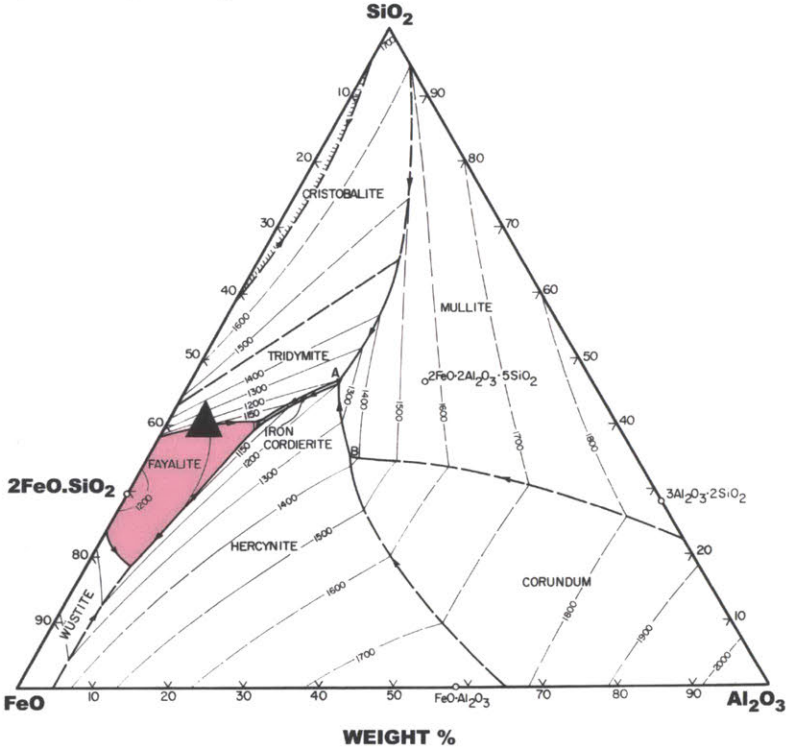

Figure 41. SiO_2 -Al_2O_3 -FeO ternary diagram - smooth clinky slag Tm plot.

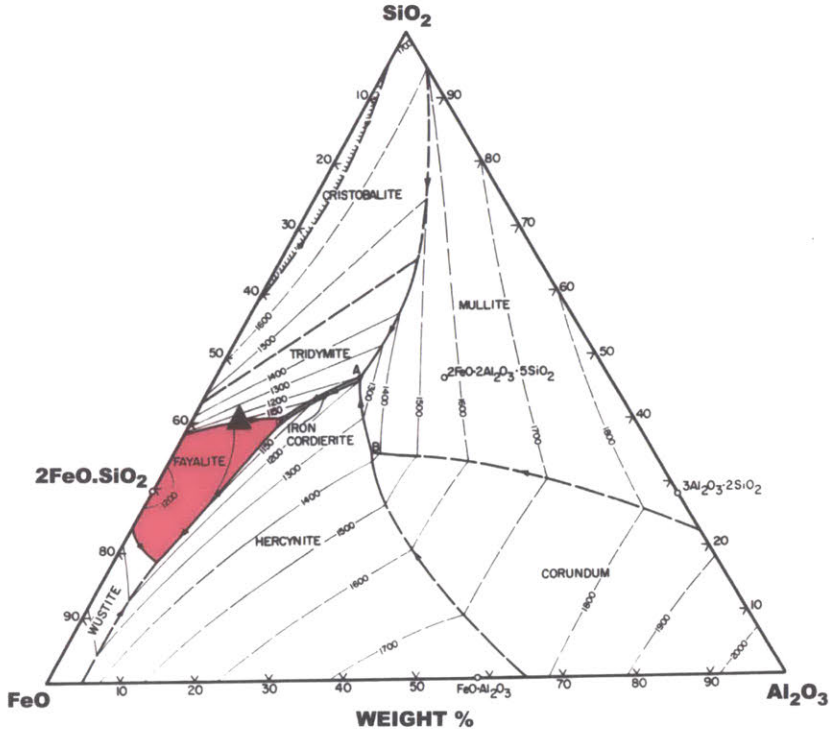

Figure 42. SiO_2 -Al_2O_3 -FeO ternary diagram - smooth non-clinky slag Tm plot.

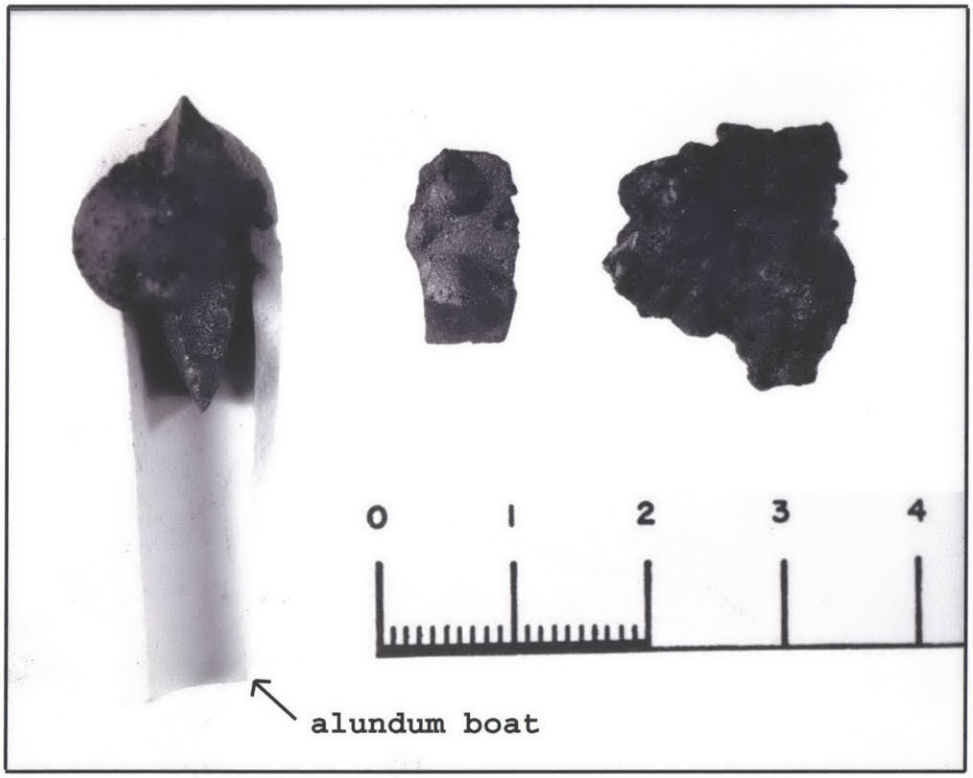

Figure 43. Assemblage of heat modified slags. Left to right: DH 2.4, DH 2.13, DH 2.14A.

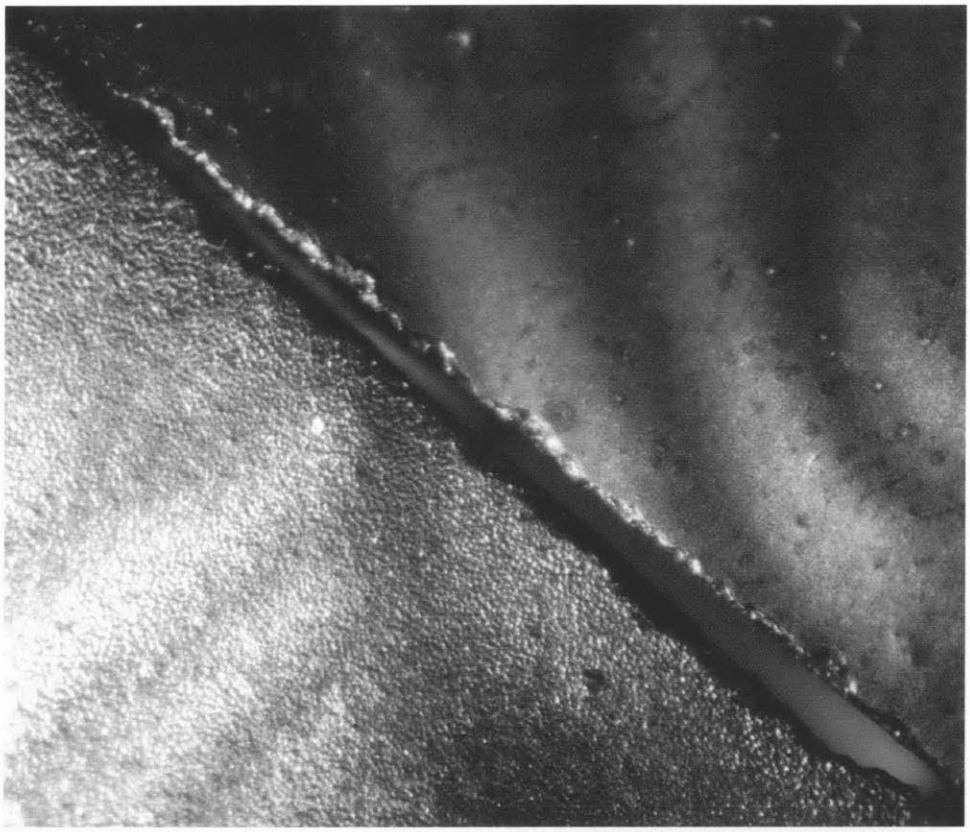

Figure 44. DH 2.13: Comparison of surfaces before and after heat modification.

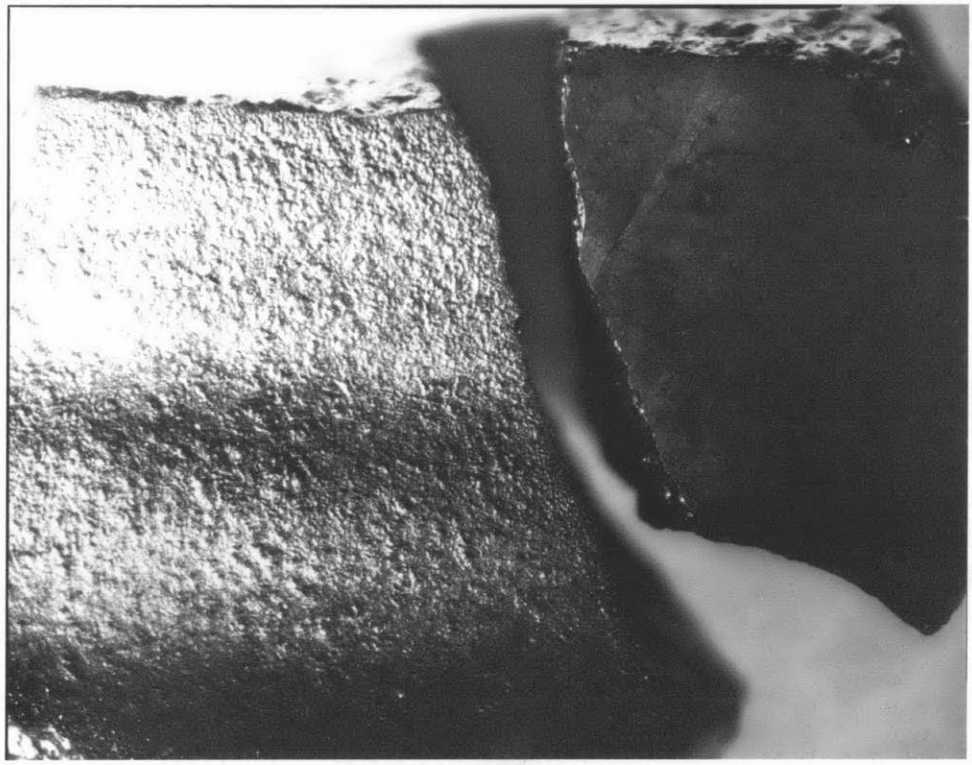

Figure 45. DH 2.17: Comparison of surfaces before and after heat modification.